BRONCHOPULMONARY DYSPLASIA, IDIOPATHIC PULMONARY ARTERIAL HYPERTENSION, AND WAVE MODELING IN STENTED VESSELS

A Senior Scholars Thesis

by

ANDREW MILTON PETERS

Submitted to the Office of Undergraduate Research
Texas A&M University
in partial fulfillment of the requirements for the designation as

UNDERGRADUATE RESEARCH SCHOLAR

April 2009

Major: Biomedical Engineering

BRONCHOPULMONARY DYSPLASIA, IDIOPATHIC PULMONARY ARTERIAL HYPERTENSION, AND WAVE MODELING IN STENTED VESSELS

A Senior Scholars Thesis

by

ANDREW MILTON PETERS

Submitted to the Office of Undergraduate Research
Texas A&M University
in partial fulfillment of the requirements for the designation as

UNDERGRADUATE RESEARCH SCHOLAR

Approved by:

Research Advisor: James E. Moore
Associate Dean for Undergraduate Research: Robert C. Webb

April 2009

Major: Biomedical Engineering

ABSTRACT

Bronchopulmonary Dysplasia, Idiopathic Pulmonary Arterial Hypertension, and Wave Modeling in Stented Vessels. (April 2009)

Andrew Milton Peters
Department of Biomedical Engineering
Texas A&M University

Research Advisor: Dr. James E. Moore
Department of Biomedical Engineering

Despite the many advances in medicine, bronchopulmonary dysplasia (BPD) remains a major obstacle for survival in neonates. Recent studies have fostered interests in the effects of hemodynamics on the disease's progression and in potential treatment strategies to optimize those effects on pulmonary vascular development. We proposed the application of a stent to alter wave phenomena in the pulmonary vasculature and utilized a monocroatiline porcine model of another pulmonary vascular disease, pulmonary arterial hypertension (PAH), to identify the hemodynamic attributes which could be altered to ameliorate the progression of these diseases. We then simulated blood flow through five, simple finite element vessel models to determine the effects of stents on wave propagation. Our porcine model showed a significant increase in the impedance moduli (|Z|), a 200% increase in the characteristic impedance (Z_C), and a 30% decrease in pulmonary vascular resistance (PVR) in the diseased subjects (n=4) compared to the controls (n=3). In our simulations, we noticed a large decrease in the |Z| and a 50-70% decrease in Z_C with the deployment of a stent. We also noticed an

increased difference in |Z| and Z_C between the upstream and downstream ends of the vessel indicating that stiffened regions of a vessel created by a stent do alter wave propagation within the vessel. In our porcine models, we concluded that the changes in the Z_C could reflect the remodeling of the pulmonary vasculature in response to the disease's progression, and, since the PVR was lower than the controls in these subjects, we hypothesized that the remodeling of the vasculature has not progressed enough to see the increase in mean pressure and PVR yet. This observation could have indicated that the disease was in an earlier stage that is synonymous with the early, undetected stages of PAH in humans. We also concluded that the small observed changes in the pressure and flow in our simulations, small size of the stent, and the current stent complications would prevent them from provoking an adequate global response to mediate the disease state and its progression.

DEDICATION

This work is dedicated to my grandparents, Russell and Francis Peters and Kenneth and Carolyn Rummel, whose hard work, love, and support have always inspired me to take on new challenges. They taught me how to face my fears, embrace the moment, and recognize the important things in life, and I am grateful for their constant influence on my life.

ACKNOWLEDGMENTS

This work was supported financially by the Undergraduate Summer Research Grant program of Dwight Look College of Engineering, the Undergraduate Research Scholars Program of the Office of Undergraduate Research, and the Vascular Biomechanics Lab of the Department of Biomedical Engineering at Texas A&M University, and I am very grateful for their financial contributions.

I am also grateful for the guidance and encouragement given by Dr. James E. Moore and other members of the Vascular Biomechanics Lab: Joao S. Soãores, Clark A. Meyer, Luke H. Timmins, Ellie Rahbar, and Will Richardson. Many thanks also go to Dr. Pierre-Henri Rolland for his support and contribution of PAH data for analysis.

As always, none of this would have been possible without the support of my family and friends. Special thanks go to my parents, Douglas and Mary Jo Peters, and my siblings, Derek, Julia, and Jana Peters, who have understood and supported all my intellectual and educational pursuits throughout my life. I must also thank my many friends and classmates for their encouragement and for all the rejuvenating distractions and breaks from my research and course work which they have provided over these last four years.

NOMENCLATURE

BPD	Brochopulmonary Dysplasia
DH	Diaphragmatic Hernia
IPAH	Idiopathic Pulmonary Arterial Hypertension
NHICHHD	National Inst. of Child Health and Human Development
NHLBI	National Heart, Lung and Blood Institute
ORD	Office of Rare Diseases
FPAH	Familial Pulmonary Arterial Hypertension
PAH	Pulmonary Arterial Hypertension
PVR	Total Pulmonary Vascular Resistance
Z_C	Characteristic Impedance
P	Pressure
Q	Flow
Z	Impedance
$\overline{P}$	Mean Pressure
$\overline{Q}$	Mean Flow
t	Time
|P|	Pressure Modulus
|Q|	Flow Modulus
|Z|	Impedance Modulus

θ_Q	Flow Phase
θ_P	Pressure Phase
P^m	Measured Pressure
P^f	Forward Propagating Pressure Waves
P^b	Retrograde Propagating Pressure Waves
Q^m	Measured Flow
Q^f	Forward Propagating Flow Waves
Q^b	Retrograde Propagating Flow Waves
E_D	Energy Delivered
P_D	Power Delivered
FEM	Finite Element Modeling
c	Wave Speed
A	Area
C	Compliance
V	Velocity of Blood
CMS	Compliance Matching Stent
CMSP	CMS-Rigid Stent Hybrid Oriented Proximally
CMSD	CMS-Rigid Stent Hybrid Oriented Distally
CS1	Control Subject One
CS2	Control Subject Two
CS3	Control Subject Three
DS1	Diseased Subject One

DS2	Diseased Subject Two
DS3	Diseased Subject Three
DS4	Diseased Subject Four

TABLE OF CONTENTS

Page

LIST OF FIGURES

LIST OF TABLES

CHAPTER I

INTRODUCTION

Despite the many recent and effective advances in the care and treatment given to preterm infants, bronchpulmonary dysplasia (BPD) and diaphragmatic hernias (DH) still foster major obstacles to infant survival. Both conditions cause major problems associated with the development and health of neonate lungs and their associated vasculature which inevitably become exacerbated following exposure to extrauterine life. These different disease conditions and their pathologies encourage research in alternative treatments for both conditions. Lately, research has broadened, advocating a focus on the development of the vasculature of fetal lungs, and the effects of the pulsatile nature of blood flow on pulmonary vasculature morphogenesis.

Recent work and studies performed by Rolland et al [1] have focused on the issue of pulsatile hemodynamics in vascular dysfunction caused by BPD and DH. The objective of the study intended primarily to investigate the effectiveness of an endothelin receptor antagonist on pulmonary perfusion and the survival of BPD/DH, preterm Merinos d'Aries lambs. The study's results concluded with possible therapeutic treatment approaches for DH and BPD that focused on the pulsatile forward and backward nature of blood flow in the fetal vasculature. This study included the concept of a filtering device designed to discourage backward flow and limit the afterload, or the return of mechanical energy, to the developing heart. Such a therapeutic device would then serve

This thesis follows the style of Journal of Biomechanical Engineering.

to encourage pulmonary development and post-natal survival [1] by reducing the workload of the heart or altering any possible physiological stimuli in the larger arteries near the heart.

If such a therapeutic device does affect the physiological environment in the upstream vessels, it could possibly be applied to other vascular diseases in which pathological signals could be altered in the larger vessels to either relieve strain or possibly slow or halt the progression of the disease and remodeling of vascular tissues. One such disease includes idiopathic pulmonary arterial hypertension (IPAH) which is a disease that affects the adult pulmonary vasculature. The causes and pathological signals which govern the progression of this fatal disease remain uncertain, but vascular remodeling plays a role in its development.

With the heterogeneity associated in vessels with implanted stents, the application of a stent poses as a possible backward wave filtering device. Our investigation into the effects of a stent's elastic properties on wave phenomena could determine whether it is rational to investigate the use of stents to alter the physiological environment in diseased vasculature.

Bronchopulmonary dysplasia and diaphragmatic hernias

The technology and care of preterm infants has come a long way since Northway and his colleagues first proposed a definition of BPD in 1967 [2,3] as a lung injury that

developed as a consequence of mechanical and oxygen ventilation. The original pathology of the disease included fibrosis, inflammation, and a lack of development in infant lungs. Current treatment practices, including the application of surfactant and more gentle ventilation techniques, have increased the chances of survival and altered the pathology and diagnosis of BPD. There have been recent efforts by groups, including the National Institute of Child Health and Human Development (NHICHHD), National Heart, Lung and Blood Institute (NHLBI), and the Office of Rare Diseases (ORD), to redefine BPD to allow physicians to better identify and diagnose it. Currently, infants suffering from BPD have become gradually younger and more fragile as the newer, improved standards and treatments have developed requiring a more current, mature definition to reflect the pathology and diagnosis of infants with BPD [2]. Recent investigations suggest that infants currently suffer less from fibrosis, and more from inflammation and abnormalities in the alveoli and the microvasculature [3], so the "new" [2] definition describing the diagnosis of BPD in infants has become focused more closely on lung tissues with impaired development caused by trauma which create adverse morphogenic responses in the premature lung tissues [2,3].

Usually BPD seen in infants is attributed to the developing tissues response to oxygen and ventilation techniques, but in the study done by Rolland and colleagues, the BPD found in the fetal lambs ensued from diaphragm hernias created by prenatal surgery. Their post procedure investigation of the lung tissue indicated abnormal lung

development consistent with the pathologic hypoplastic lungs, seen in many cases of DH, and inadequate vasculature development [4].

Idiopathic pulmonary arterial hypertension (IPAH)

Pulmonary hypertension is a vascular disease defined by an increase in the vascular pressure (>25 mmHg at rest or >30 mmHg during increased activity) [5,6] of the normally low pressure, high flow vasculature of the lungs. An increase in vascular resistance of the pulmonary tree caused by constriction of the downstream vessels leads to the development of the elevated blood pressure. The constriction is related to the vascular remodeling of the vessels in response to various stimuli. This increase in resistance places a larger after load on the heart as it moves blood through the pulmonary vasculature eventually leading to right ventricular dysfunction and failure [7].

In many cases pulmonary hypertension is a secondary disease caused by another underlying pathological condition, however IPAH is not linked to other diseases or conditions, and its cause is uncertain. Research has recently associated this condition to chemical, environmental, and genetic factors, and, as a result, the disease has been further classified into familial pulmonary arterial hypertension (FPAH - more predominantly linked to genetic factors and family history) and IPAH [7,8]. The incidence of IPAH is not currently known, but there are approximately 300 new cases a year in the United States with a tendency toward women between the ages of 21 and 40 and a median survival of 2.8 years [7,9]. Diagnosis of IPAH proves difficult in the

clinical setting because many of its symptoms closely correlate to other cardiovascular and pulmonary diseases, and all other possibilities must be ruled out prior to its diagnosis. Current treatments for IPAH alleviate the symptoms and slow the progression of the disease however no cure exists, and the average length of survival for a patient diagnosed with IPAH is only three years [10].

Current research into IPAH revolves around genetic factors, vasoactive compounds, cellular signaling, and the cellular pathways that lead to the development of pulmonary vascular remodeling. Since a low clinical occurrence of IPAH exists, a number of experimental models have been developed to study the different factors that attribute to FPAH and IPAH which include hypoxic and chemically induced pulmonary hypertensive animal models [8,11].

Wave propagation in human vasculature

An abundance of wave phenomena can be observed in a variety of periodic events which occur in nature and our modern world. The idea of a wave can be easily conveyed to most people with a guitar string or waves in a puddle, but waves can also be found in more complex systems such as those found in biology. Blood flow and the human vascular tree is a prime example of wave propagation in a complex, physiological system as the energy generated by the heart pulses through the vascular tree propelling blood through the various tissues of the body. This pulse of energy can be felt at various points in the body at different times, and, as an example, can be best experienced

with simultaneous arterial pulse measurements taken at the carotid and radial artery where the slight time difference in the arrival of the pulse can be felt by any observer.

Now, to better visualize this propagating pulse of mechanical energy, one can imagine a blood vessel as a long tube filled with fluid and extend this image to two different, simplified cases. In the first case, we could assume that the fluid in the tube is compressible while tube is long and rigid. If we apply a force to a piston which encloses the fluid at one end of the tube or similarly add a small amount of liquid at the enclosed end, a compressed segment of the fluid would propagate down the tube in a longitudinal fashion similar to sound traveling through air or a compression in a slinky. Alternatively, we can consider fluid in the tube as incompressible and assume we have an elastic tube which dilates in response to an increase in pressure. In this case, when we apply the same force with the piston or add the same amount of fluid, a segment of the tube would dilate in response to the increase in pressure. The dilated vessel segment would then travel down the tube in a transverse manner similar to a wave traveling on a string propelling blood with it.

These ideas of wave travel in simple fluid models can be extended to blood flow in the viscoelastic blood vessel with the heart supplying the force of the piston or excess fluid. However, when we expand this idea of a traveling wave from a vessel to a vascular tree, we must begin to consider wave reflections and changes in the media through which a wave is traveling. As with other waves, any change in the medium will return a certain

amount of energy as a reflection which can create a significant amplification. If this amplification is difficult to understand, consider for an example, sound waves produced by a dog barking in an enclosed room. Assuming the walls are not too thick, anyone passing by the room could hear the muffled dog bark as the sound waves traverse through the walls of the room to the individual, but, for anyone in the room, the barking would be louder than normal because the dog's bark would echo off the walls. In this situation, only a portion of the energy of the dog's bark passes from the air into the much denser wall while the rest reflects back away from the wall into the room. An individual inside the room then hears the accumulation of the reflected sound waves and the initial bark amplifying the noise.

Thus, in the same way that the change from air to solid wall reflects a portion of a sound wave, any changes in a vessel, such as changes in radius, stiffness, or geometric path (e.g. bifurcations), would also cause a reflection, and, with the numerous bifurcations and vessel changes in a human vascular tree, there are a number of wave reflections which accumulate with every beat of the heart. In the body, this accumulation of wave reflections contribute to the oscillatory, AC, component of blood flow and can form a significant return of energy to the heart which creates a resistive force against which the heart must drive blood.

The wave equation and wave speed

The wave equation for blood flow though a vessel can be derived from a Eularian perspective of flow through a segment of an artery. Assuming that the vessel is a straight compliant tube with an inviscid fluid and assuming the wave speed is much larger than blood velocity, we can begin with Euler's equation for flow:

$$\frac{\partial u}{\partial t} + u\frac{\partial u}{\partial x} = \frac{-1}{\rho}\frac{\partial p}{\partial x} \qquad (1)$$

where u is the blood velocity, t is time, x is the length down the vessel, ρ is the density of the fluid, and p is pressure. By nondimmensionalizing u, we can reduce Euler's equation to

$$\frac{\partial u}{\partial t} = \frac{-1}{\rho}\frac{\partial p}{\partial x} \qquad (2)$$

Then applying the conservation of mass, we find

$$\frac{\partial (Au)}{\partial x} = 0 \qquad (3)$$

where A is the cross sectional area of the vessel. We can then derive the wave equation assuming small deformations by finding

$$\frac{\partial^2 r}{\partial x^2} = \frac{2\rho k}{r}\frac{\partial^2 r}{\partial t^2} \qquad (4)$$

where r is the radius and k is a constant that describes the small deformation in radius in response to changes in pressure $(\partial r / \partial p)$. Expanding on this idea, we next apply the law of Laplace and assume that the vessel wall is linearly elastic to derive Moens-Kortweg equation for wave speed, c:

$$c = \sqrt{\frac{Eh}{2r\rho}} \qquad (5)$$

where E is the elasticity of the vessel and h is the thickness of the vessel wall [12,13].

When solving the wave equation with any given c, we would be looking for a solution, U, similar to d'Alembert's solution for a traveling wave:

$$U(x,t) = A(x + \alpha \cdot t) + B(x - \alpha \cdot t) \qquad (6)$$

which can be found by applying the proper initial and boundary conditions to the given wave problem [14,15].

Stents

In America's modern healthcare, cardiovascular disease remains a major health concern afflicting an estimated 80.7 million people in the United States with high blood pressure, coronary artery disease, stroke, or heart failure. Atherosclerosis, a progressive disease in which the build of plaque leads to an occlusion of the vessel, has proven to be a major contributor in the development and progression of cardiovascular disease [16], and a variety of endovascular treatment options exist for patients including arterial bypass, stenting, balloon angioplasty, and endovascular aneurysm repair [17].

In simple terms, a stent can be considered a rigid cage designed to prop open an occluded blood vessel to restore blood flow through an artery and provide support as the vessel heals following balloon angioplasty. During balloon angioplasty, a cardiologist

threads a catheter with a balloon tip through the arterial tree to the site of the occlusion where the balloon is inflated to push open the plaque and vessel wall to reestablish blood flow. This procedure places increased mechanical stress on the vessel potentially damaging the vessel and leading to a variety of complications including reocclusion. The placement of a stent in the reopened vessels seeks to decrease the occurrence of this problem by providing a scaffold to support the vessel as it heals following the procedure.

Stenting comes with its own disadvantages and complications. The placement of a foreign, metallic stent in an artery elicits a normal immunological response in the body which includes inflammation, thrombosis, and smooth muscle cell proliferation, and this response can lead a variety of complications including restenosis [18,19] of the vessel which would require an additional procedure to reopen or restent the vessel. Thus, a lot of investment has been placed into stent design and implementation.

Advances in stent design include the development of drug eluting stents which release chemicals designed to locally suppress the body's immune response, yet research also goes into the mechanical properties of stent designs with the intent to develop new stents which optimize the beneficial mechanical properties of the stent while minimizing the mismatch between the stent and the surrounding vessel hopefully decreasing the magnitude of the immunological response and reduce the chance of reocclusion and failure [18,19].

The filter concept

The placement of a stent within a vessel doesn't just evoke an immune response; it also alters the mechanical properties of a vessel. The presence of the rigid cage of a stent within a vessel creates a vessel segment which contrasts the viscoelastic arterial tissue around it while also changing the stresses and strains placed on the vascular tissue. This heterogeneity alters the local characteristics of the vessel thereby modifying the medium through which a pulse wave travels in the vessel. It is this property in which our investigation is focused as we question whether or not this stiffened region of vascular tissue serves to resist or alter the return of backward flow within the human vasculature or whether it conceals any higher frequency signal content, measured in pressure and flow, which could possibly alter physiological stimuli or signals.

CHAPTER II

METHODS

Since the intent of this investigation was to determine whether or not the application of a stent serves to alter any physiological signals or reduce the return of the backward propagating waves within the human vasculature, we needed to identify the presence or characteristics of backward propagating waves or pathological signals within the human vasculature by hemodynamically investigating the pathological conditions of a pulmonary vascular disease. We also needed to establish a simple analytical model to predict the effect of a stent on wave propagation in the simplest situation. This model could then serve as a foundation for future evaluation should our results warrant further investigation. The hemodynamic analysis of the vascular disease should also couple the two parts of our investigation by providing a methodical approach to analyze the stent models and quantify any induced changes in the presence of a stent.

PAH analysis

Though the idea of the application of a wave filtering device evolved from the evaluation of the pathological hemodynamics associated with BPD/ DH vasculature, the accessibility and analysis of the PAH test data proved to be more beneficial to this study. The PAH data and evaluation was provided by Rolland and colleagues, and it consisted of pressure and flow data of an adult porcine, PAH model. In the model, PAH was induced by delivering monocrotaline into the pulmonary artery. Data from four diseased animals and three control animals were used to analyze the impedance and reflected

waves of the pathological condition. The data were obtained in two multiple sets with the diseased measurements taken three months after PAH was induced. Data from the control subjects were obtained over a period of approximately 20 seconds. The data obtained from four diseased animals were collected for 8 to 9 seconds. All measurements were taken at a rate of 500 Hz.

Data from the individual cardiac cycles was isolated by two different methods. In the first data set, pressure and flow had been synchronized with the ECG measurements. Thus, we defined and separated each beat from R peak to R peak given the ECG. Any abnormalities in the ECG, pressure, or flow measurements were avoided in our analysis. In the second data set, ECG measurements were not included so we isolated each beat using the foot of the pressure wave. Given measurement quality and consistent periodicity, we chose five to six heart beats from each of diseased subjects for analysis from approximately the same time intervals (e.g. the first, second, or third complete beat in each second). A nearly identical approach was taken for the control data except that we chose more beats for a larger control group.

Using Fourier analysis, pressure and flow data from each isolated beat was analyzed in the frequency domain using mathematical software (MATLAB R2006B, Version 7.3.0, The MathWorks). We chose to leave the phase angle of each harmonic unwrapped so their values would not be restricted to the range between $-\pi$ and π. The characteristic

impedance (Z_C) and pulmonary vascular resistance (PVR) was calculated through the application of Ohm's law,

$$Ze^{i\omega t+\theta_Z} = \frac{Pe^{i\omega t+\theta_P}}{Qe^{i\omega t+\theta_Q}} \qquad (7)$$

where P is pressure, Q is flow, Z is the impedance, ω is the frequency, and θ is the phase. The PVR was determined by the mean pressure ($\overline{P}$) over the mean flow ($\overline{Q}$), the magnitude of the impedance (|Z|) at each frequency was determined by dividing the pressure magnitude by the flow magnitude, and the phase was determined by subtracting the flow phase (θ_Q) from the pressure phase (θ_P). The characteristic impedance (Z_C) was computed by averaging the second through tenth harmonics.

We isolated the forward and backward wave components in the time domain with the measured pressure (P^m), measured flow (Q^m), $\overline{P}$, $\overline{Q}$, and Z_C following the methods described by Westerhof et al [13] and Quick et al [20] thereby isolating the AC component of the measured pressure and flow waves from the DC component using

$$\dot{P} = P^m - \overline{P} = P^f + P^b \qquad (8)$$

$$\dot{Q} = Q^m - \overline{Q} = Q^f + Q^b \qquad (9)$$

$$P^f = \frac{\dot{P} + Z_C \cdot \dot{Q}}{2} \qquad (10)$$

$$P^b = \frac{\dot{P} - Z_C \cdot \dot{Q}}{2} \qquad (11)$$

$$Q^f = \frac{P^f}{Z_C} \qquad (12)$$

$$Q^b = \frac{-P^b}{Z_C} \qquad (13)$$

where $\dot{P}$ and $\dot{Q}$ are the oscillating or AC components of pressure and flow, and P^f, P^b, Q^f, and Q^b are the forward and backward wave components of pressure and flow, respectively.

Since the value of Z_C used in these calculations was determined from the measured magnitude of each harmonic, this calculation gives us a real value to use in the time domain. However, it should be noted that this calculation neglects blood viscosity and the viscoelasticity of the pulmonary vascular tree [13]. Fig. 1 provides a summary of the calculations necessary for each beat in our analysis to determine the results of the experiment.

The energy delivered (E_D) to the pulmonary vasculature and the power delivered (P_D) by the heart was also evaluated for each beat

$$E_D = \int_0^T P(t) \cdot Q(t) dt \qquad (14)$$

$$P_D = \overline{P} \cdot \overline{Q} \qquad (15)$$

The mean and standard deviation of P, Q, PVR, Z_C, E_D, and P_D was calculated for each animal and reported as such (± SD), and we used the independent, heteroscedastic t-test of unequal sizes to compare the P, Q, $\overline{P}$, $\overline{Q}$, PVR, Z_C, E_D, and P_D of the diseased and control animals to each other. P values of 0.05 were required to be considered

significantly different. Averages for the controls and diseased animal sets were determined from the individual beats.

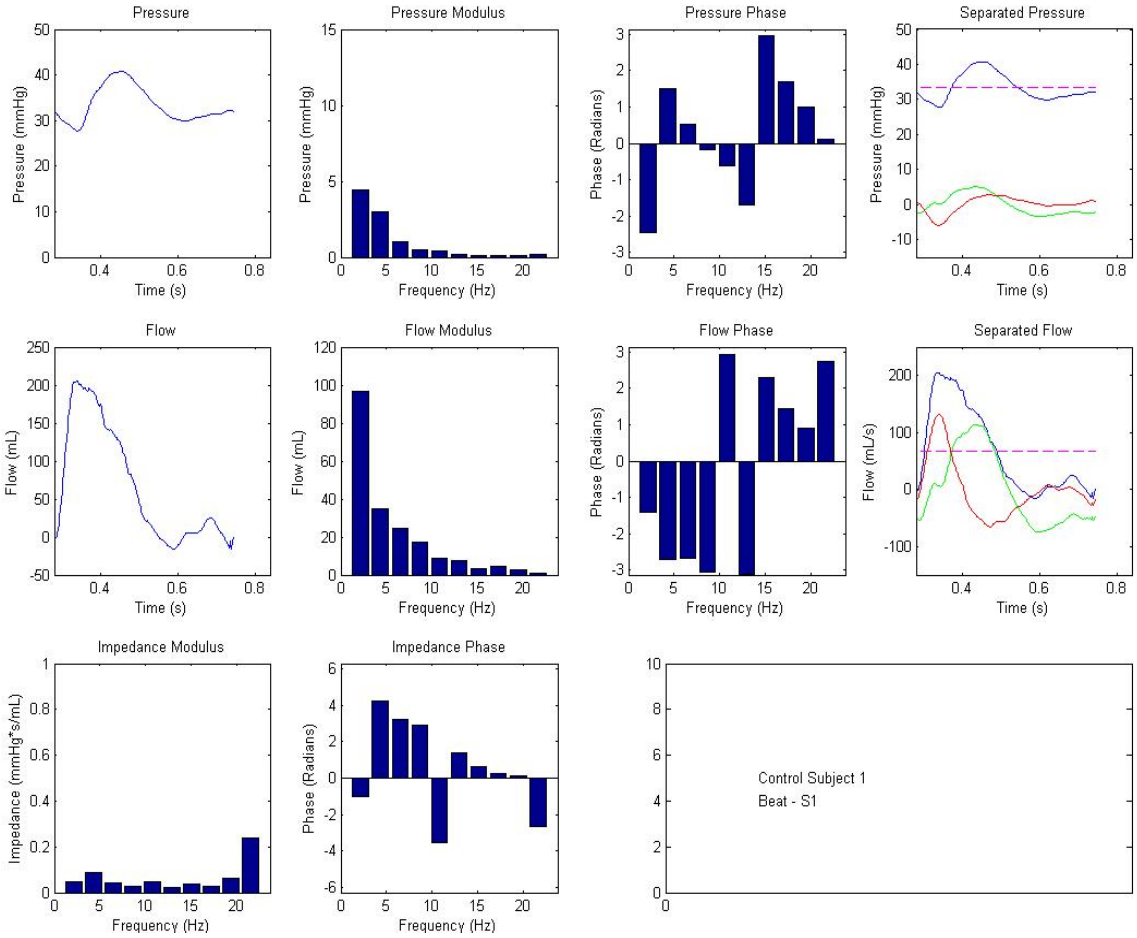

Fig. 1 Sample Summary of Our Frequency and Time Domain Analysis. This figure provides a brief summary of the frequency and time domain results of our data analysis. Using P and Q measurements, the modulus and phase of the P and Q wave forms can be determined in the frequency domain. These are then used to calculate the Z modulus and phase. Z moduli are utilized to calculate the Z_C which allows us to separate the measured waves into their forward and backward running components.

Finite element vessel model

The finite element method has been used in numerous applications to model and predict various physiological systems in biomechanics [21,22] including stent applications

within vessel models [18,19]. Finite element modeling (FEM) appeared to be the best method to create our simple model allowing us to focus on the properties of the stent within a vessel so we could identify any changes in wave propagation in the simplest case. We built an FEM software program using MATLAB R2006b, Version 7.3.0 expanding upon ideas and software methods used in previous stent investigations. The calculating routines and function files were developed in parallel for five different vessel 1-D models, and the models differed only in the application of the different stent designs applied to each vessel.

Though a variety of methods have been used to adequately model blood vessels and the human vasculature, we chose the simple, linear 1-D wave equation to model blood flow hoping to emphasize the wave like nature of blood flow within a vessel. Thus extending Eq. 4, I used

$$\frac{\partial^2 Q}{\partial t^2} = c^2 \frac{\partial^2 Q}{\partial x^2} \qquad (16)$$

where the wave speed, c, is defined by Eq. 5.

Attempting to imitate some of the anatomical dimensions of the larger pulmonary arteries, I utilized vessel properties estimated from literature [23] to construct five frictionless tubes attached to a pump which stimulates flow at the origin, ($Q(0,t)$), and at the outlet to a long frictionless tube intended to provide an escape for the fluid while stimulating a small resistive force to create a reflected wave. The properties assigned to

the vessel created a wave speed near ~2 m/s which was consistent with the slower wave speeds found within the larger arteries of the pulmonary vascular system. The vessel properties used in the model can be found in Table 1.

Table 1 Defined Dimensions and Properties Used in Test Models. The dimensions are very small and have been determined given literature [23] and with infant pulmonary vasculature values in mind.

	Length (cm)	Internal Radius (cm)	Wall Thickness (cm)	Elastic modulus (dynes/cm^2)	c_0 – Wave Speed (m/s)	Total Model Length (cm)
Model 1 – Control Model (No Stent)						
Vessel	5	0.18	0.078	15	1.751	5
Model 2 – Stent Design 1						
Vessel	4	0.18	0.078	15	1.751	5
Transition Region (2)	0.45	0.18	0.088	15 - 150	1.751 - 5.537	
Rigid Region	0.1	0.18	0.088	150	5.537	
Model 3 – Stent Design 2						
Vessel	4	0.18	0.078	15	1.751	5
Transition Region (2)	0.8	0.18	0.088	15 – 150	1.751 - 5.537	
Rigid Region	0.2	0.18	0.088	150	5.537	
Model 4 – Stent Design 3						
Vessel	4	0.18	0.078	150	1.751	5
Transition Region	0.8	0.18	0.088	15 – 150	1.751 - 5.537	
Rigid Region	0.2	0.18	0.088	150	5.537	
Model 5 – Stent Design 4						
Vessel	4	0.18	0.078	15	1.751	5
Rigid Region	1	0.18	0.088	150	5.537	

In order to test the simple design under various flow conditions and flow rates, I defined the action of the pump as a sinusoidal function, ($g(t)$). We tested the flow at rates of 4 Hz and 3 Hz to better compare its results with those seen in an earlier set of data from the porcine models of our corresponding PAH investigation with two different sinusoidal functions, ($g_1(t)$) and ($g_2(t)$).

In our simulation, the long frictionless tube at the end of the model was defined as

$$\frac{\partial Q}{\partial t}(l,t) = w(l,t) = 0 \qquad (17)$$

where *w(l,t)* is constant, and the vessel began at a zero state condition defined by

$$Q(x,0) = f(x) = 0 \qquad (18)$$

$$\frac{dQ(x,0)}{dt} = h(x) = 0 \qquad (19)$$

From there we incremented time steps to calculate the amount of flow located at each node within the vessel model using the 1-D, time dependent solutions calculated by

$$\{\ddot{u}_0\} = [M^2]^{-1}(\{F_0\} - [K]\{u_0\}) \qquad (20)$$

$$[M^2]\{\ddot{u}\} + [K]\{u\} = \{F\} \qquad (21)$$

$$\{\ddot{u}\}_{s+1} = a_3(\{u\}_{s+1} - \{u\}_s) - a_4\{\dot{u}\}_s - a_5\{\ddot{u}\}_s \qquad (22)$$

$$\{\dot{u}\}_{s+1} = \{\dot{u}\}_s + a_2\{\ddot{u}\}_s + a_1\{\ddot{u}\}_{s+1} \qquad (23)$$

where *M*, *K*, and *F* represent FEM matrices calculated using quadratic elements and the wave equation. u , $\dot{u}$, and $\ddot{u}$ represent the solution and its time derivatives at each point within the model, and the coefficients a_1, a_2, a_3, a_4, and a_5 constitute stability and accuracy parameters defined by

$$a_1 = \alpha \cdot \Delta t \qquad (24)$$

$$a_2 = (1-\alpha) \cdot \Delta t \qquad (25)$$

$$a_3 = \frac{2}{\gamma \cdot (\Delta t^2)} \qquad (26)$$

$$a_4 = \frac{2}{\gamma \cdot (\Delta t)} \qquad (27)$$

$$a_5 = \frac{1}{\gamma - 1} \qquad (28)$$

where Δt is the change in time and α and γ are two parameters assigned the values of 3/2 and 8/5, respectively, for the Galerkin method [24].

Of the five vessel models, we used one as the control and placed three generic stent designs into the other four models. All three simplified, 10 mm long designs were placed 2 cm from the origin of their vessel models altering the properties of their respected vessels at those locations. At the most rigid locations of the stent the elasticity of the vessel increased by a factor of ten, and, at other locations in the stented regions, a linear transition function was utilized to describe the elasticity. The intent of our transition model was to simulate the effect of a compliant matching stent [19].

Fig. 2 shows the three different stent designs in their respected orientations within their designated vessel models. As shown, we utilized the basic concept of the compliance matching stent (CMS) with a transition region at both ends where the elasticity was defined as a function of the location, $E_1(x)$, with a rigid reinforced center. We also utilized a uniform rigid stent to create sharp contrasts at both ends of the stent within the vessel model. We then created a hybrid of the two models and oriented the compliant end proximally or distally to the origin. These two models denoted CMSP (proximal orientation) and CMSD (distal orientation) had values for elasticity defined by another function, $E_2(x)$.

Using the same linear, frictionless assumptions applied to the vessel model, I calculated the pressure at each location in the vessel model utilizing space and time derivatives and assuming that vessel deformations were small compared to the radius of the vessel given

$$\frac{dP}{dt} = -\frac{A}{C}\frac{dV}{dx} \qquad (29)$$

$$\frac{dV}{dt} = -\frac{1}{\rho}\frac{dP}{dx} \qquad (30) \quad [25]$$

$$V = \frac{Q}{A} \qquad (31)$$

where P is pressure, A is the area at mean pressure, C is compliance of the tube, and V is the velocity of blood.

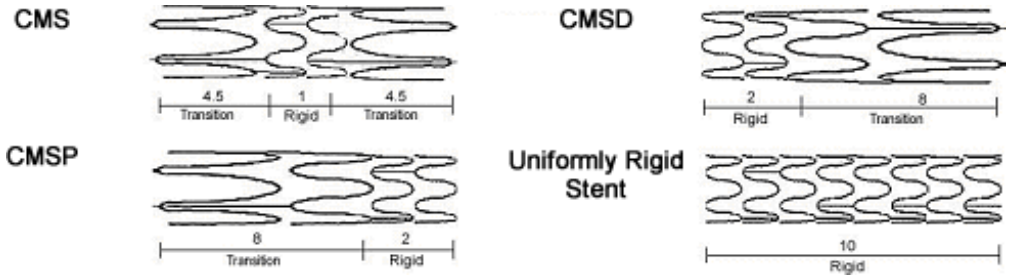

Fig. 2 Generic Stent Model Designs. The four stent designs are generic, conceptualized models designed to imitate the elastic properties of a compliance matching stent (CMS) and a uniformly rigid stent. CMSP and CMSD are hybrid designs of the uniformly rigid and CMS stent with the compliant end oriented proximally to the origin (CMSP) and distally to the origin (CMSD). The origin of the model would be located to the left of each design and the vessel outlet would be located to the right. Dimensions are in mm.

Using pressure and flow measurements taken at five different locations in each vessel model (Fig. 3), the pressure, flow, and the impedance of the vessel models could be evaluated using the same methods used to evaluate the PAH animal models. Again, the

measured waves were decomposed into the DC and the forward and backward AC components, and the impedance, energy, and power of each system were compared.

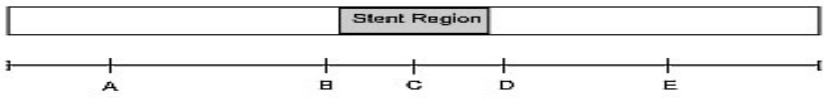

Fig. 3 Approximate Measurement Positions of the 5 cm Test Models. Position A is located 1 cm from the origin. Positions B and D are located 1 mm before and after the region of the vessel where the different stent models were located. Position E is located 4 cm from the origin and Position C is located in the middle of the vessel model.

CHAPTER III

RESULTS

Hemodynamic PAH results

Analysis of the time averaged parameters revealed that $\overline{P}$ was significantly higher in the controls compared to the diseased animals. In the controls, $\overline{P}$ was 34.1±2.0 mmHg compared to 19.8±2.4 mmHg in the diseased (Table 2). More variation was seen between the diseased animals as they ranged from 18.8 mmHg to 23.1 mmHg compared to 32.4 mmHg to 36.9 mmHg in the control. Time averaged $\overline{Q}$ in the controls was slightly higher than the diseased animals, but the difference was not significant. The diseased animals had a $\overline{Q}$ of 51.9±16.1 mL/s compared to 59.9±15 mL/s in the controls. More variation was present in both sets of data as $\overline{Q}$ in CS1, CS2, and CS3 ranged between 40.02±2.3 mL/s and 74.26±3.2 mL/s in CS2 and CS3, respectively, and $\overline{Q}$ rates fell between 78.27±2.2 mL/s and 33.63±0.56 mL/s in DS1 and DS4, respectively. Though no significant difference was present between the average $\overline{Q}$ of the Controls and the Diseased, individually $\overline{Q}$ in DS1, DS2, DS3, and DS4 showed significant difference from the controls.

The magnitude of the pulsatile pressure components (|P|) indicated that the diseased subjects had a significantly higher |P| than the controls in the first and second harmonics. The |P| in the diseased subjects was also significantly higher after the fourth harmonic.

Table 2 Summary of Hemodynamics of Porcine PAH Study. * indicates values which were significantly different from the averages (AVG) seen in the controls.

SUBJ	$\overline{P}$ (mmHg)	$\overline{Q}$ (mL/s)	Z_C $\left(\frac{mmHg \cdot s}{mL}\right)$	PVR $\left(\frac{mmHg \cdot s}{mL}\right)$
CS1	33.0 ±0.2	65.3±2.4	0.0540±0.024	0.506±0.019
CS2	32.4±0.2	40.0±2.3	0.0634±0.018	0.811±0.046
CS3	36.9±0.2	74.3±3.2	0.0516±0.0091	0.498±0.022
AVG	34.1±2.0	59.9±15	0.0563±0.018	0.605±0.15
DS1	18.8±0.1*	78.3±2.2*	0.072±0.016	0.240±0.0061*
DS2	16.6±0.2*	44.1±3.0*	0.0994±0.024*	0.378±0.023*
DS3	20.4±0.1*	52.5±1.8*	0.112±0.008*	0.390±0.013*
DS4	23.1±0.2*	33.6±0.56*	0.390±0.052*	0.688±0.015*
AVG	19.8±2.4*	51.9±16.1	0.169±0.13*	0.423±0.17*

As shown in Fig. 4, there was a large amount of deviation in the diseased subjects. However, closer observation indicated that the increased magnitude in the first harmonic is largely due to DS4 whose magnitude was more than double (>10 mmHg) that of DS1, DS2, and DS3 (<= 5 mmHg). A similar observation was made in the second harmonic, but there were no significant differences between the control and diseased subjects in the second harmonic.

The flow magnitude (|Q|) in the frequency domain, shown in Fig. 5, was higher in the control subjects throughout the first ten harmonics, and the differences were significant in all but the third harmonic. Similarly to |P|, a larger deviation was also present in the first harmonic in the diseased set, but the deviation couldn't be contributed to only one animal perhaps reflecting the differences in $\overline{Q}$ seen between the diseased animals.

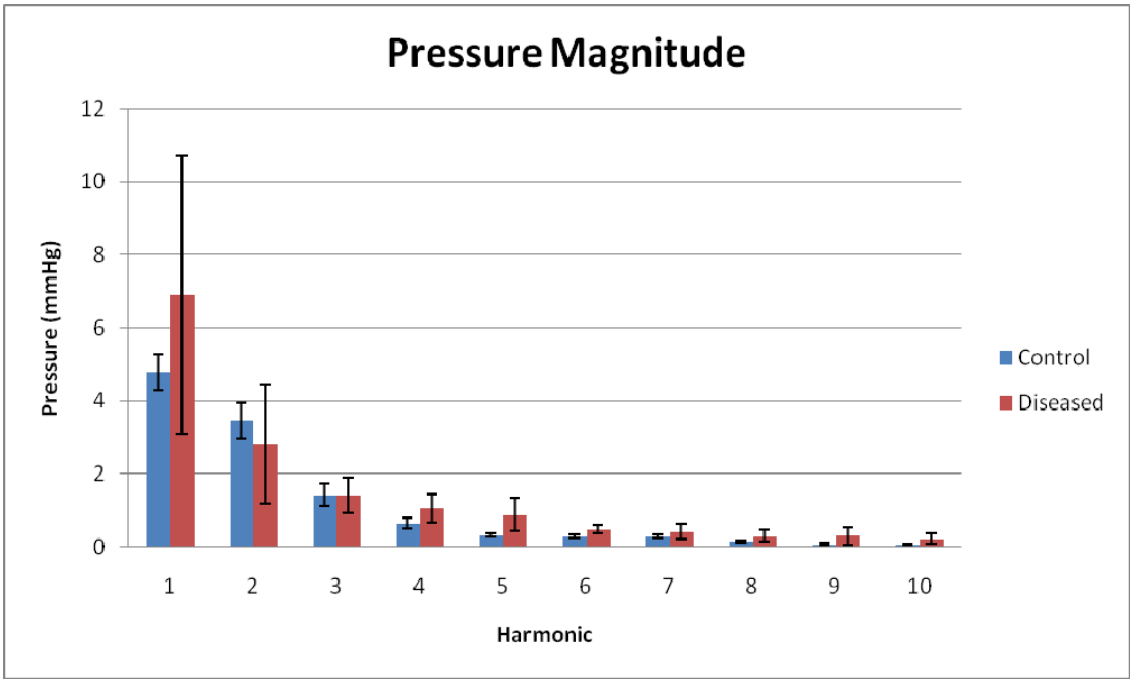

Fig. 4 Pressure Magnitude in the Frequency Domain. The diseased subjects (red) had higher P magnitudes in the first and higher harmonics than the control (blue). The diseased subjects deviated more from animal to animal than the control, and the deviation was more pronounced in the lower harmonics.

PVR was significantly higher in the control subjects compared to the diseased subjects. The PVR in the control subjects was 0.605±0.15 mmHg*s/mL compared to 0.423±0.17 mmHg*s/mL. The PVR did vary from animal to animal however. The values of $\overline{P}$ and $\overline{Q}$ resulted in the PVR's of 0.506±0.019 mmHg*s/mL, 0.811±0.046 mmHg*s/mL, and 0.498±0.022 mmHg*s/mL for CS1, CS2, and CS3, respectively, while DS1, DS2, and DS3 had values of 0.240±0.0061 mmHg*s/mL, 0.378±0.023 mmHg*s/mL, and 0.390±0.013 mmHg*s/mL which were all significantly different. DS4 was higher than the control average at 0.688±0.015 mmHg*s/mL and was significantly different.

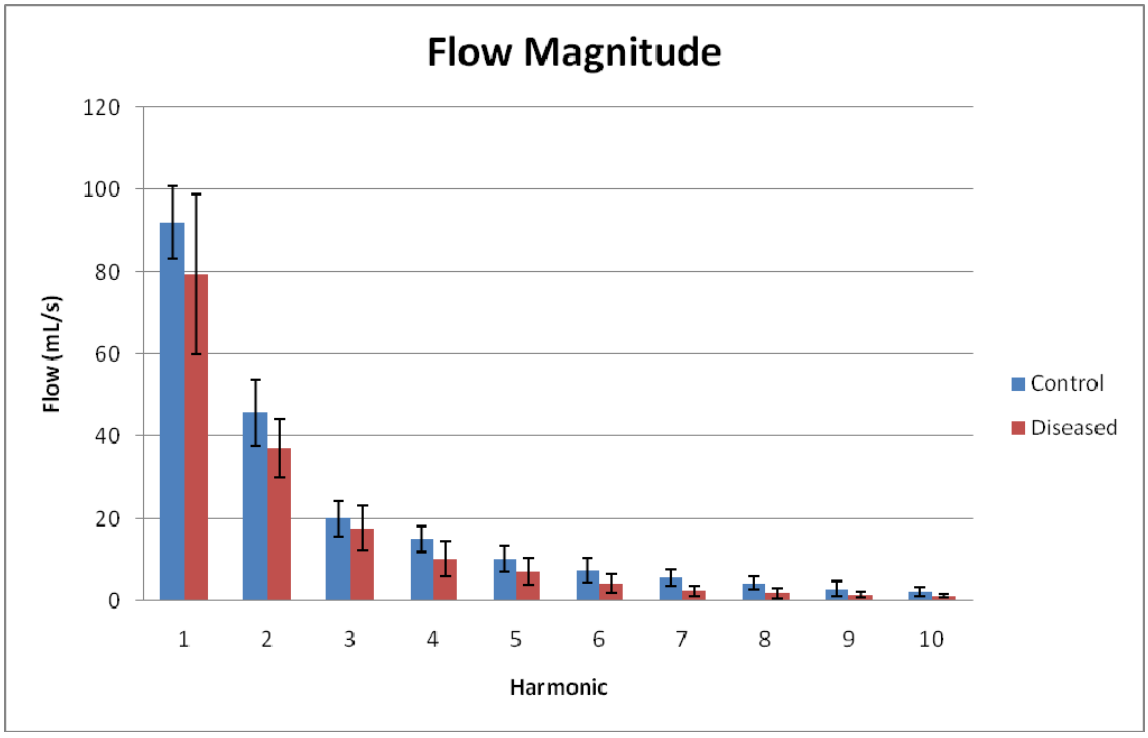

Fig. 5 Flow Magnitude in the Frequency Domain. The control subjects (blue) had higher Q magnitudes than the diseased subjects (red), but not significantly. The deviation appeared to be comparable in both subjects. However, it is slightly larger in the diseased subjects.

The diseased group exhibited a higher impedance magnitude (|Z|) in the first ten harmonics in the frequency domain and the difference increased significantly after the third harmonic. As shown in Fig. 6, the higher |Z| values had higher standard deviation values associated with them. The standard deviation also increased with frequency in the controls as well. Closer observation of the |Z| showed that DS4 tended to have the highest |Z| of the diseased subjects. However, DS1, DS2, and DS3 still had higher |Z| values than the controls. The higher |Z| values contributed to the significantly higher Z_C in the diseased subjects compared to the controls. Individually, DS2, DS3, and DS4 all had significantly higher Z_C than the controls, but the increase was not significant in DS1. The differences in PVR and Z_C are summarized in Table 2.

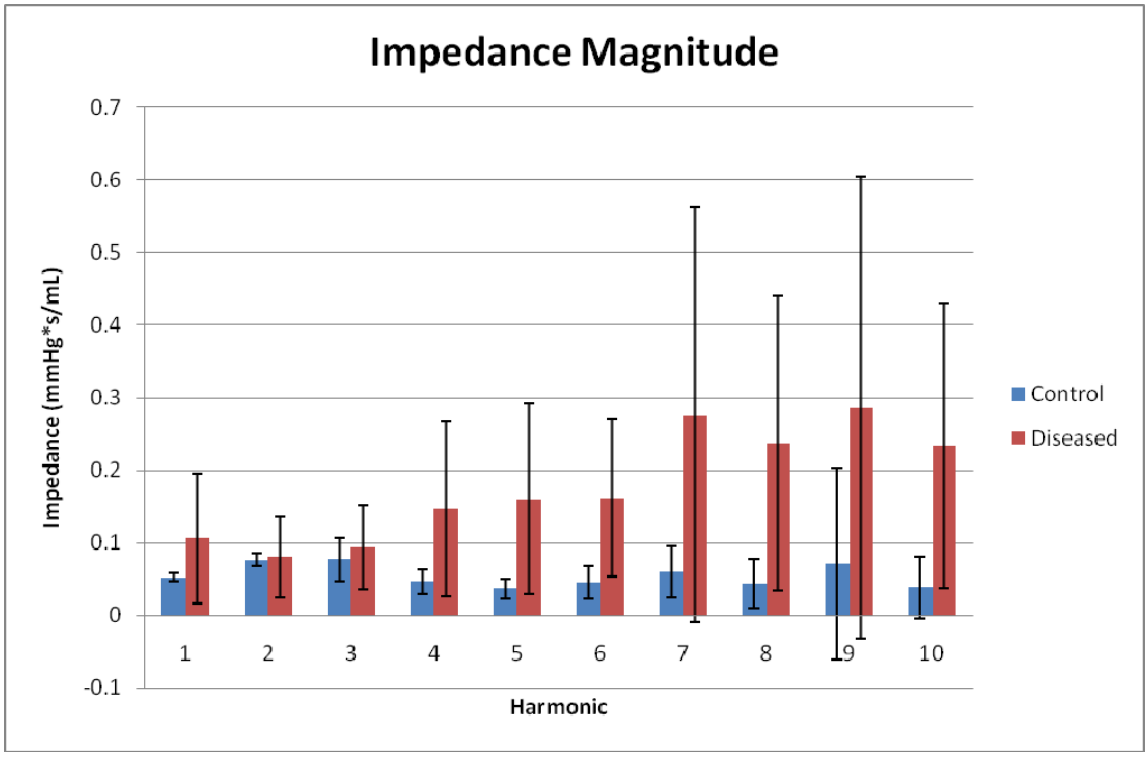

Fig. 6 Impedance Magnitude in the Frequency Domain. The diseased subjects (red) had higher Z magnitudes than the diseased subjects (red). The increased impedance his higher at higher frequencies, but the deviation increases at higher frequency as well. The increased |Z| reflects the increased Z_C expected in hypertension.

In all three controls shown in Fig. 7, the anterograde waves reached a maximum at peak or near peak systolic pressure (P), and retrograde waves hit a minimum at peak flow (Q) when P was only beginning to increase. The diseased animals were different from the controls as the maximum anterograde value and minimum retrograde values occurred nearly simultaneously at peak systole. Also, the retrograde waves reached a maximum later in diastole in DS1, DS2, DS3, and DS4 than in the controls. These maxima in the diseased then tended to be at or near the resting diastolic retrograde wave values in DS1,

DS2, and DS3. In the CS1, CS2, and CS3, the retrograde waves achieve a maximum value right after the anterograde peaked in late systole/ early diastole.

The consistent P and Q profiles in CS1, CS2, and CS3, provided consistent forward (anterograde) and backward (retrograde) wave decompositions in the time domain. Meanwhile in the diseased animals, shown in Fig. 8, the anterograde and retrograde waves were consistent in each respective animal but not between animals. The consistency in the controls reflected the lower deviation and smaller ranges seen in the measurements of the controls. They also reflected a baseline condition of healthy animals rather than the various conditions of the diseased animals. The various differences in the conditions of the diseased animal were the most obvious in the differences in between DS1 and DS4. DS1's measured and retrograde waves contrast those of DS4 which are both distinct. In fact, with the exception of DS4, the retrograde waves in the diseased animals tended to be much flatter than the controls.

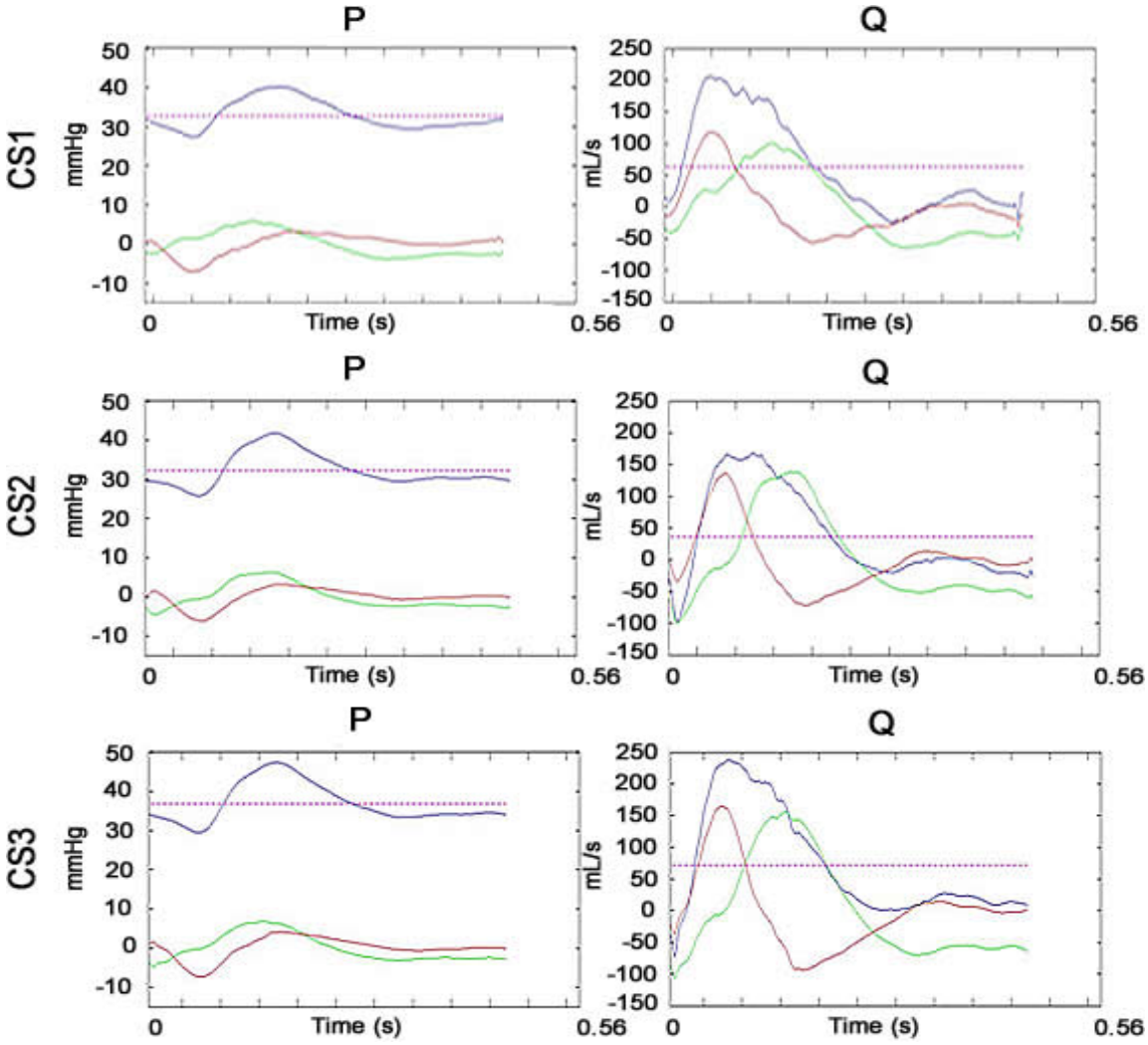

Fig. 7 Separated Forward and Backward Waves in the Control Subjects. Typical measured P and Q (blue) beats of CS1, CS2, and CS3 showed little variation between beat. The forward propagating waves (green) appear to peak later at peak systolic P, while retrograde waves (red) reach a minimum early in systole peaking at peak Q. The retrograde waves attain a maximum value during late systole/ early diastole at nearly the same time as peak P and maximum forward propagating waves. In addition to the mean values (dashed pink) the retrograde and anterograde waves compose the measured wave. A shoulder could be seen in measured P prior to peak systole along with a standard exponential decay that ended with a slight increase in measured P midway through diastole. The increase coincided with the second hump seen in measure Q. Each had a period of approximately 0.5 seconds.

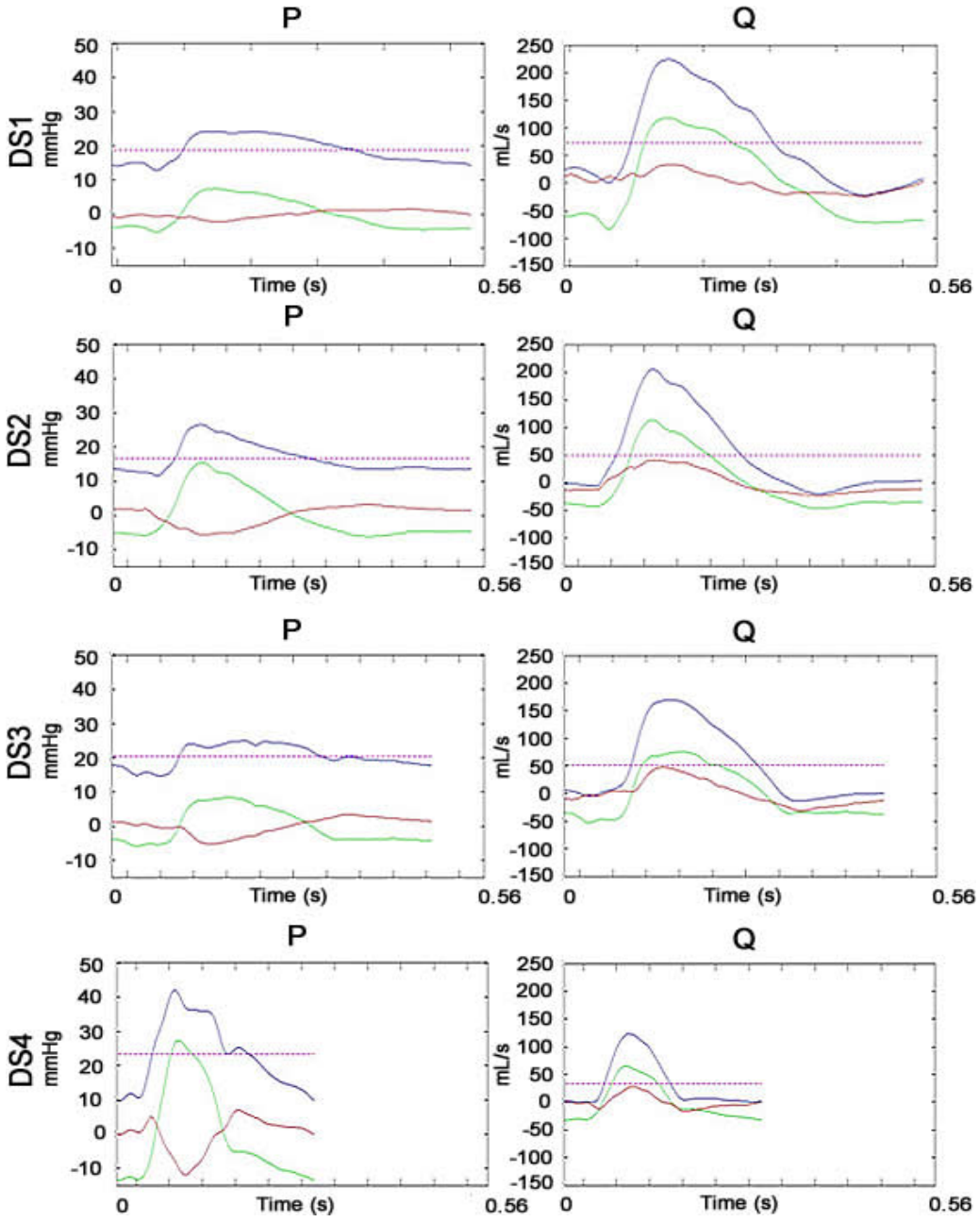

Fig. 8 Separated Forward and Backward Waves in the Diseased Subjects. Typical measured P and Q (blue) beats of DS1, DS2, DS3, and DS4 showed more variation between each animal than the control. The forward propagating waves (green) appear to arrive at peak systole along with the retrograde wave (red) minimum. The retrograde maximum occurs later in diastole than in the controls, and the maximum appeared to be at or near a consistent retrograde diastolic value. These two waves in addition with the mean value (dashed pink) compose the measured wave. The shoulder seen in measured P prior to peak systole in the control subject isn't present. The measured P profiles in DS1 and DS3 where much broader and flatter than the controls. DS2 looks the most similar of the diseased subjects to the control subjects. It appears the increased BPM in DS4 could have influenced its measured P profile, and it could be related to the diminished Q.

Measured P in each of the controls had a shoulder prior to peak systole which was not present in the diseased animals. This shoulder reflected the arrival of peak Q in the control. The peak Q in the diseased animals arrived at peak P thus there was no shoulder. Measurements in the P and Q in the diseased and control animals also differed in the diastolic exponential decays. The control animals displayed similar exponential decays with a slight rise in diastole. In P, the decay ended midway through diastole and coincided with the second hump also seen in the Q measurements. In DS1 and DS3, the P waves didn't show this attribute and were instead much broader and flatter than any of the controls. Meanwhile, DS2 had a sharper peak with a more pronounced decay than the other DS1 and DS3 animals and even showed a small hump similar to the controls. However, DS4 was different than the other diseased and control animals. It had a large systolic increase and a quick decay into another beat. This occurrence was most likely the result of a decreased period and increased heart rate to compensate for decreased Q.

Of note in each animal was that Q led P. Q wave shapes were also similar between the diseased and control animals despite different $\overline{Q}$ values. One irregularity was noticed in CS2, but may have been due to noise in these measurements. The noise tended to be more pronounced at the foot of the Q wave which, in this case, caused a global minimum.

The hearts of the control subjects appeared to deliver more P_D to the pulmonary vasculature than their diseased counterparts (Table 3). The hearts of CS1, CS2, and CS3 delivered 592.5±22.8, 371.6±21.3, and 764.1±33.0 mW which was significantly higher than all of the diseased subjects. Of the diseased subjects, DS2's heart delivered the least amount of power with only 137.2±8.7 mW per beat on average, and DS1's heart delivered the most amount of power at 235.6±5.8 mW per beat. It was also notable that DS4's increased heart rate allowed it to deliver 210.3±81.8 mW. DS3 delivered 166.5±5.2 mW.

Table 3 Energy and Power Summary of Hemodynamics in the Porcine PAH Study. * indicates values which were significantly different from the averages (AVG) seen in the controls.

SUBJ	Heart Rate (bpm)	P_D (mW)	E_D (mJ)
CS1	125	592.5±22.8	140.7±5.2
CS2	127	371.6±21.3	87.2±4.9
CS3	127	764.1±33.0	179.9±6.9
AVG	127±2.1	576.1±164	136.0±39
DS1	111*	235.6±5.8*	126.9±3.2
DS2	111*	137.2±8.7*	75.9±2.7*
DS3	125*	166.5±5.2*	79.5±2.5*
DS4	201*	210.3±81.8*	46.8±0.50*
AVG	129±38.5*	181.9±48*	81.7±29*

The increased, consistent heart rates in the controls seemed to make up for some of the differences in E_D per beat between the diseased and control animals, but E_D was still higher in the controls. CS1, CS2, and CS3 delivered 140.7±5.2 mJ, 87.2±4.9 mJ, and 179.9±6.9 mJ, respectively, at a consistent heart rate of 126.6±2.1 beats per minute (BPM). DS1, DS2, DS3, and DS4 on the other hand delivered 126.9±3.2 mJ, 75.9±2.7 mJ, 79.5±2.5 mJ, and 46.8±0.50 mJ, respectively, at a hear rate of 128.9±38.5 bpm. More specifically, DS1 delivers more energy per beat than CS2, but with less beats per

minute (111 bpm versus 127 bpm) it delivers less power. DS4 delvers a lot of power at the highest heart rate (201 bpm), but it can't compensate for the little amount of E_D . DS2 had one of the lowest heart rate (111 bpm) and the second lowest E_D hence it had the lowest P_D.

Stented wave model results

The changes associated with different stent designs

The deployment of a stent reduced the amplitude differences between the upstream and downstream ends in the idealized vessel model, and also had a minor effect on the arrival times of the Q and P waves. The unstented control model (Control) had an increase in amplitude in the primary wave from point B, 1 mm proximal of the stent, to point D, 1 mm distal of the stent (see Fig. 3). The amplitude of this primary wave increased from point B to point D by 34.9% in P and 14.3% in Q (Fig. 9). The uniformly rigid stent provoked a substantial decrease in the difference in amplitudes between point B and point D, with a change of 6.8% in P and 2.5% in Q. The compliance matching stent (CMS) model gave similar reductions of 8.4% and 3.1% between point B and point D in P and Q, respectively. The rigid-compliant hybrid model with the compliant end oriented proximally to the origin (CMSP) similarly showed a 14.3% and 5.4% amplitude reduction in P and Q, respectively. The rigid-compliant hybrid model with the compliant end oriented distally to the origin (CMSD) differed slightly from our other hybrid model with a 9.7% and 3.7% change from point B to point D in P and Q, respectively.

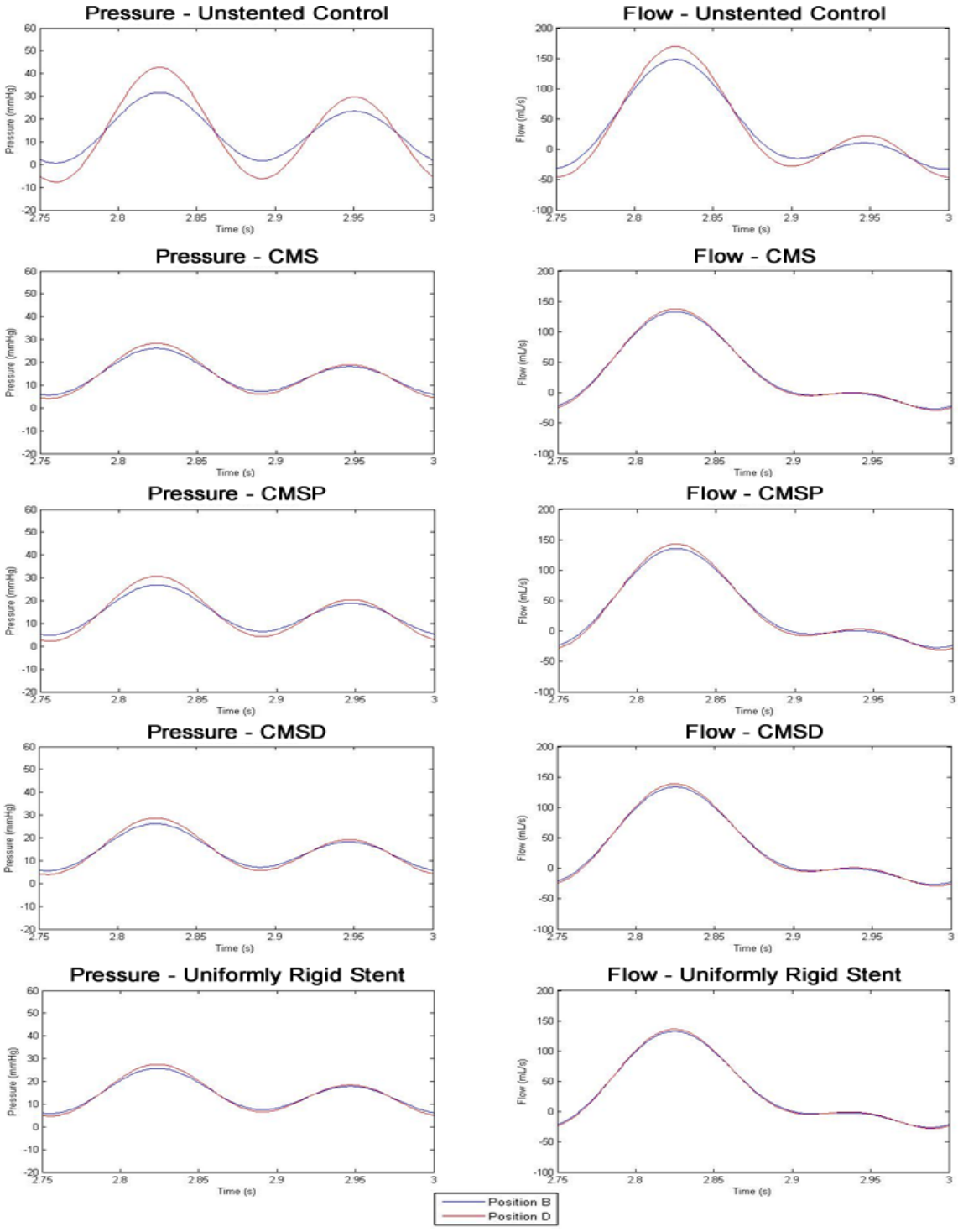

Fig. 9 Pressure and Flow Waveforms in the Simulated Vessels. Given a stimulated cosine input, the P and Q profiles in our stented models all showed a diminished amplitude in P and Q at point B (blue) and point D (red) compared to the unstented model. The stents also make the difference in amplitude between point B and point D smaller.

An inspection of the arrival times showed that the local maxima of P and Q in all of our stented models were within 0.016 s of the arrival time of the unstented control. The global maxima (the maxima associated with the larger, primary waves) seen in both P and Q occurred 0.002 s later in the unstented model compared to all of the stented models, and there was no difference in arrival time between the uniformly rigid stent, CMS, CMSP, or CMSD. The second, local maximum yielded slightly different results, but the peak values still occurred earlier in all of the stented models. Overall, the waves propagated faster in the stented models with peak P occurring 0.004±0.001 s earlier and peak Q occurring 0.010±0.0034 s earlier. These changes were expected but small given our model size and the calculated wave speeds shown in Table 1.

The relationship in time between peak P and peak Q by a Δt was zero in the primary wave but not the secondary wave. However, the second peak had a different Δt in each model, and the Δt differed at point B and point D. The unstented model had the smallest Δt with only 0.005 s between peak P and Q while the CMS model had the largest Δt with 0.018 s at point B. The CMS also had the largest difference in Δt between point B and point D of any of the models, possibly indicating that it more substantially decoupled the upstream and downstream ends of the vessel.

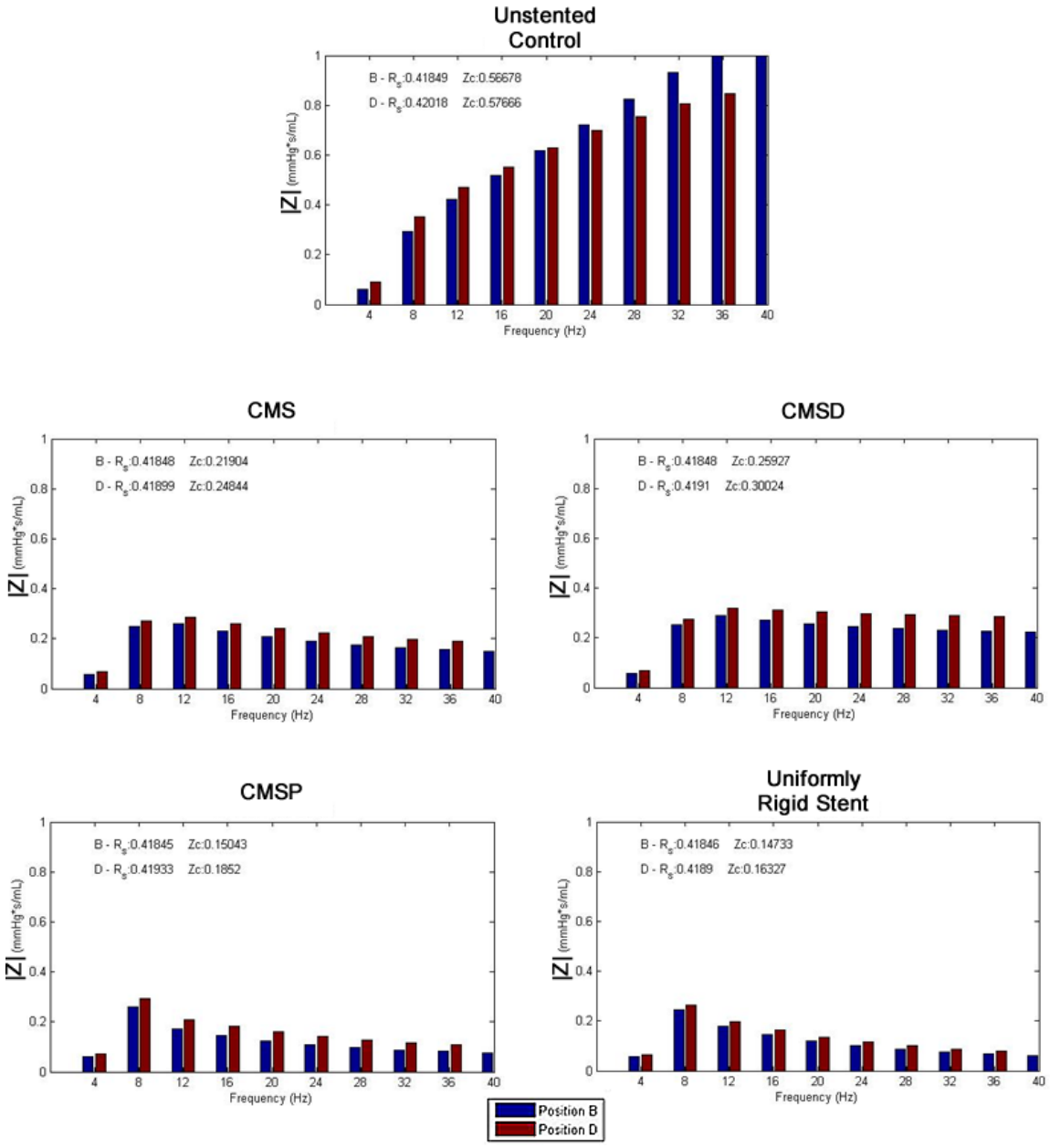

Fig. 10 Calculated |Z| in the Simulated Vessels. The presence of a stent within a vessel decreased the |Z|. The stents also altered the relationship between the proximal |Z| and distal |Z|. The amount each stent affected the |Z| can be observed in the differences in Z_C.

In our frequency analysis, it became evident that the stents not only decreased the |Z| of the vessel, each design also altered the relationship between the apparent |Z| at the upstream and downstream ends which could indicate a wave filtering capability. In our

unstented model, shown in Fig 10, the |Z| increases with frequency with |Z| being higher at point D below 24 Hz and point B above 24 Hz. This changed with the application of a stent as all four stent models maintained a much lower |Z| than the unstented control after the first harmonic. The stented models also maintained a lower |Z| at point B than point D. The uniformly rigid stent |Z| peaked at 8 Hz before decreasing throughout the rest of the first ten harmonics while the CMS model's |Z| increased up to 12 Hz before decreasing similarly. The hybrid models, CMSP and CMSD, also give similar results with CMSP mirroring the uniformly rigid stent model and CMSD mirroring the CMS.

Summarizing the changes in |Z| of all the models, our calculations indicated that the stents would change the relationship between the Z_C of the upstream and downstream ends (Summarized in Table 4). In the unstented model, the Z_C of the vessel is 1.7 % lower at point B compared to point D. The application of a uniformly rigid stent increases this difference to 9.8% while the CMS increases it even more to 12%. These changes indicated in these two models are further amplified in hybrids. In addition the hybrids indicated that the orientation of the compliant end can have an impact. The CMSD model indicates that Z_C is 14% lower at point B compared to point D and this difference increased to 19% in CMSP.

Table 4 Summary of the Difference in Z_C at Positions B and D in Computer Models. Measurements are in mmHg*s/mL. The presence of a stent and the presence or orientation of a compliant region within a stent affect the relationship between P and Q and changes the Z_C.

Characteristic Impedance, Z_C (mmHg*s/mL)	Unstented Control	CMS	CMSP	CMSD	Uniformly Rigid
Point B	0.56678	0.21904	0.15043	0.25927	0.14733
Point D	0.57666	0.24844	0.18520	0.30024	0.16327

The application of a pure cosine stimulus

Applying a pure cosine wave to our stent models reflected the results of our original calculated amplitudes, but it didn't reflect the changes in impedance. The changes in amplitude can be best summarized by Fig. 11, where one can discern the overall decrease in amplitude of the primary and secondary waves with the application of the CMS. This same result was observed with each of the stent designs. However, the change to a pure cosine stimulus at the origin did cause a change in impedance in each model. Summarized by Fig. 12 and Table 5, the apparent |*Z*| decreased in the unstented control model but increased in each of the stented models. The |*Z*| of each subject also stayed relatively constant throughout the first ten harmonics. In the end, these |*Z*|'s resulted in an observed 25% decrease in Z_C of the unstented control model and a 140%, 59%, 119%, and 32% increase in the Z_C of the uniformly rigid stent, CMS, CMSP, and CMSD models taken at point D in the first and second set of simulations, respectively. With this noticeable change, we also observed a decrease in the difference in Z_C of the proximal and distal measurement sites. The unstented model had a Z_C that was 10% lower at point B than point D. This value decreased to 3.7%, 4.3%, 6.4%, and 4.9% in the uniformly rigid stent, CMS, CMSP, and CMSD models, respectively.

Table 5 Summary of the Differences in Z_C at Position B and D in Cosine Simulations. Measurements are in mmHg*s/mL. The little change observed in |Z| indicated almost no change in Z_C.

Characteristic Impedance, Z_C (mmHg*s/mL)	Unstented Control	CMS	CMSP	CMSD	Uniformly Rigid
Point B	0.38339	0.37723	0.37944	0.37779	0.37682
Point D	0.42715	0.39435	0.40556	0.39714	0.39124

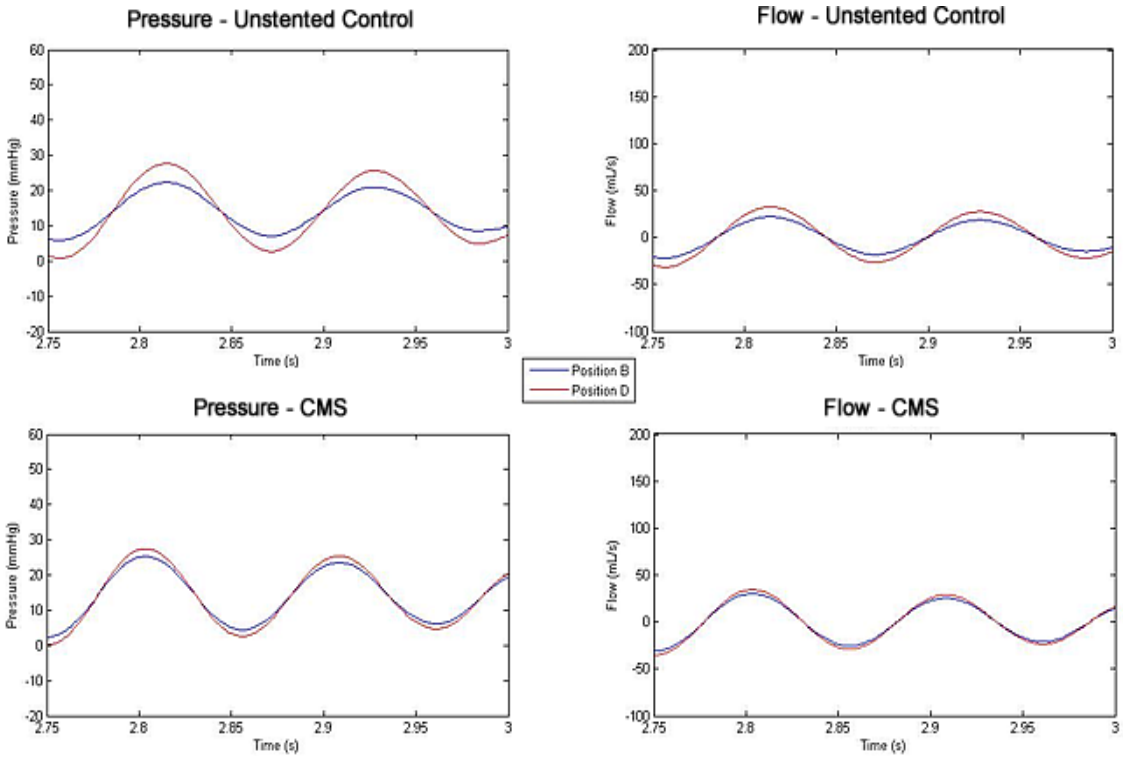

Fig. 11 Pressure and Flow Waveforms in Cosine Simulations. Given a stimulated cosine input, the P and Q profiles in our stented models all showed a diminished amplitude in P and Q at point B and point D compared to the unstented model. The stents also make the difference in amplitude between point B and point D smaller.

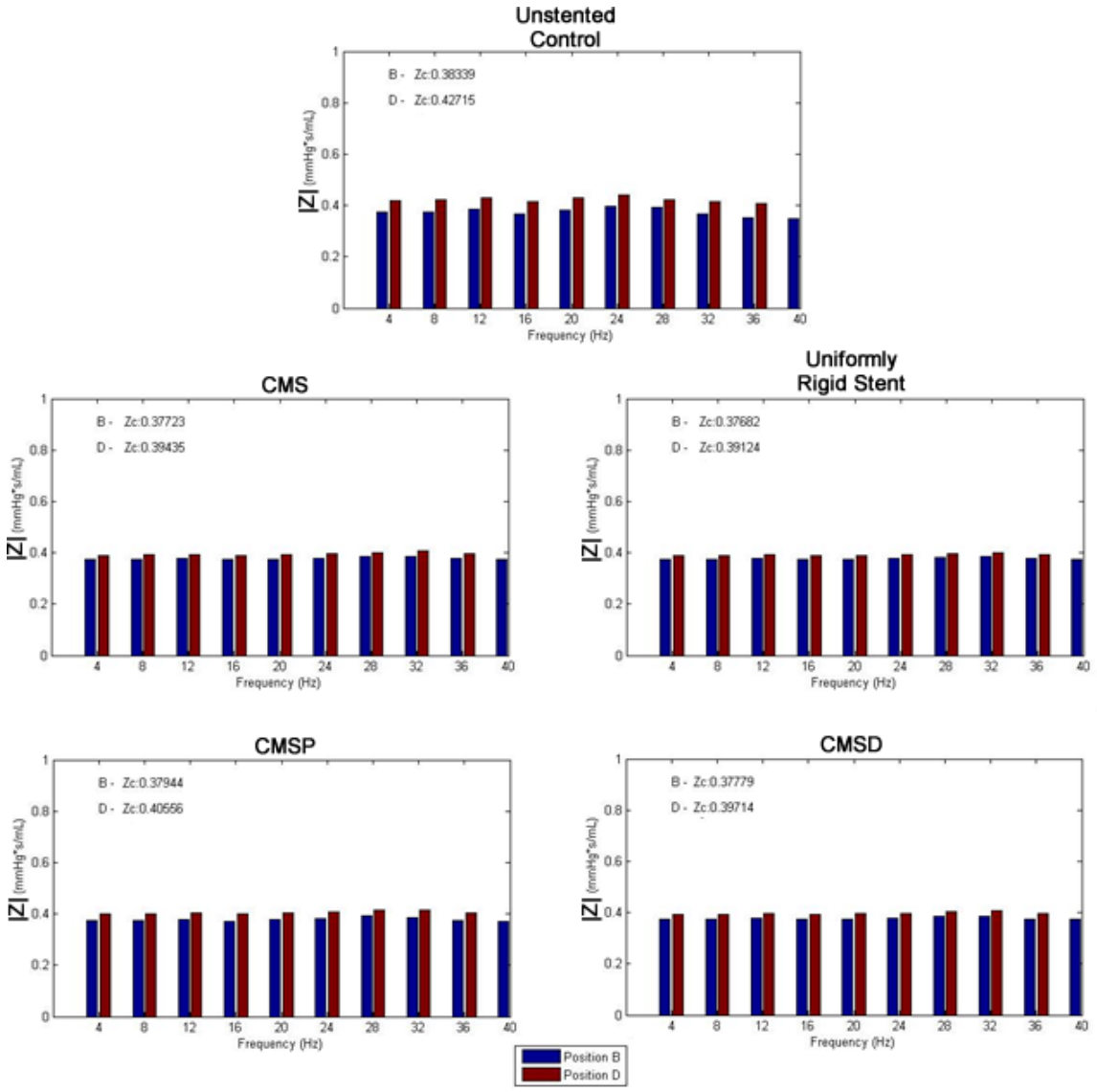

Fig. 12 Calculated |Z| in the Cosine Simulations. The presence of a stent in a vessel given a simplified cosine wave stimulus indicate that a stent had no effect on |Z|.

The effects of stent relocation

The result of moving a stent upstream and applying a similar Q wave yielded changes in amplitude and Z_C similar to those observed in our first simulations. The changes in amplitude can be best summarized by the changes observed between our unstented

control model and the CMS model shown in Fig. 13. Each of the models indicated that the stent decreased the amplitude of P and Q in a way similar to what is seen between the unstented control and the CMS model. We also observed similar changes in |Z| as the models demonstrated a decrease in |Z| after the first harmonic with a stent design present. Consequently, these |Z|, shown in Fig. 14, led to an overall decrease in Z_C compared to the unstented control. However, given these similarities, the simulations indicated that there were changes between the Z_C measured at point B and point D between this simulation and the first simulation. This indicated that the stent's location in reference to the origin had an influence on the |Z|. Summarized in Table 6, the Z_C increased compared to the first simulations at point B and point D in the uniformly rigid stent model and the CMSD model. The Z_C also increased at point B and point D in the CMS and CMSP models, respectively, but the Z_C decreased at point D and point B in these same models, respectively.

Table 6 Summary of the Difference in Z_C at Positions B and D in Relocated Stent Simulations. Measurements are in mmHg*s/mL. The stents decreased the Z_C compared to unstented control, and the Z_C's changed in comparison to the first simulations. Values which increased are highlighted in red and values that decreased are highlighted in blue.

Characteristic Impedance, Z_C (mmHg*s/mL)	Unstented Control	CMS	CMSP	CMSD	Uniformly Rigid
Point B	0.56678	0.18163	0.15276	0.19905	0.11194
Point D	0.57666	0.25534	0.16960	0.28777	0.14520

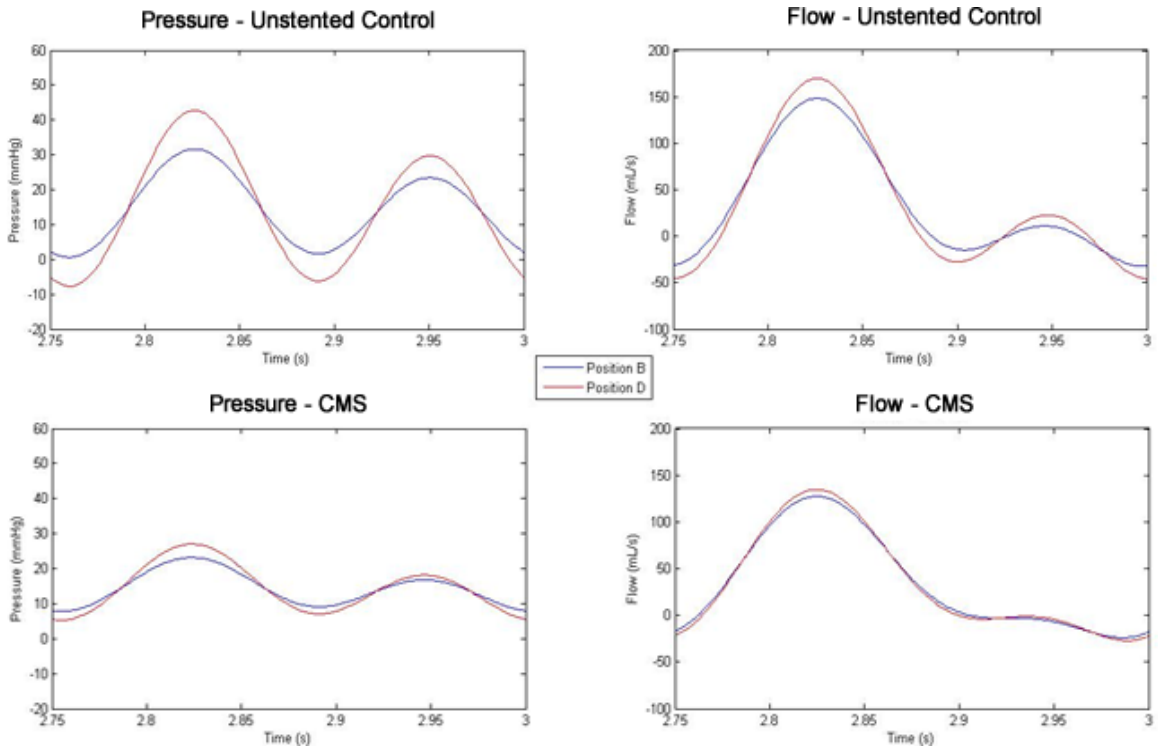

Fig. 13 Pressure and Flow Waveforms in Relocated Stent Simulations. The P and Q profiles in the stented models indicate that the amplitude of P and Q at point B and point D were diminished compared to the unstented control model. The difference in amplitudes between point B and point D were also decreased.

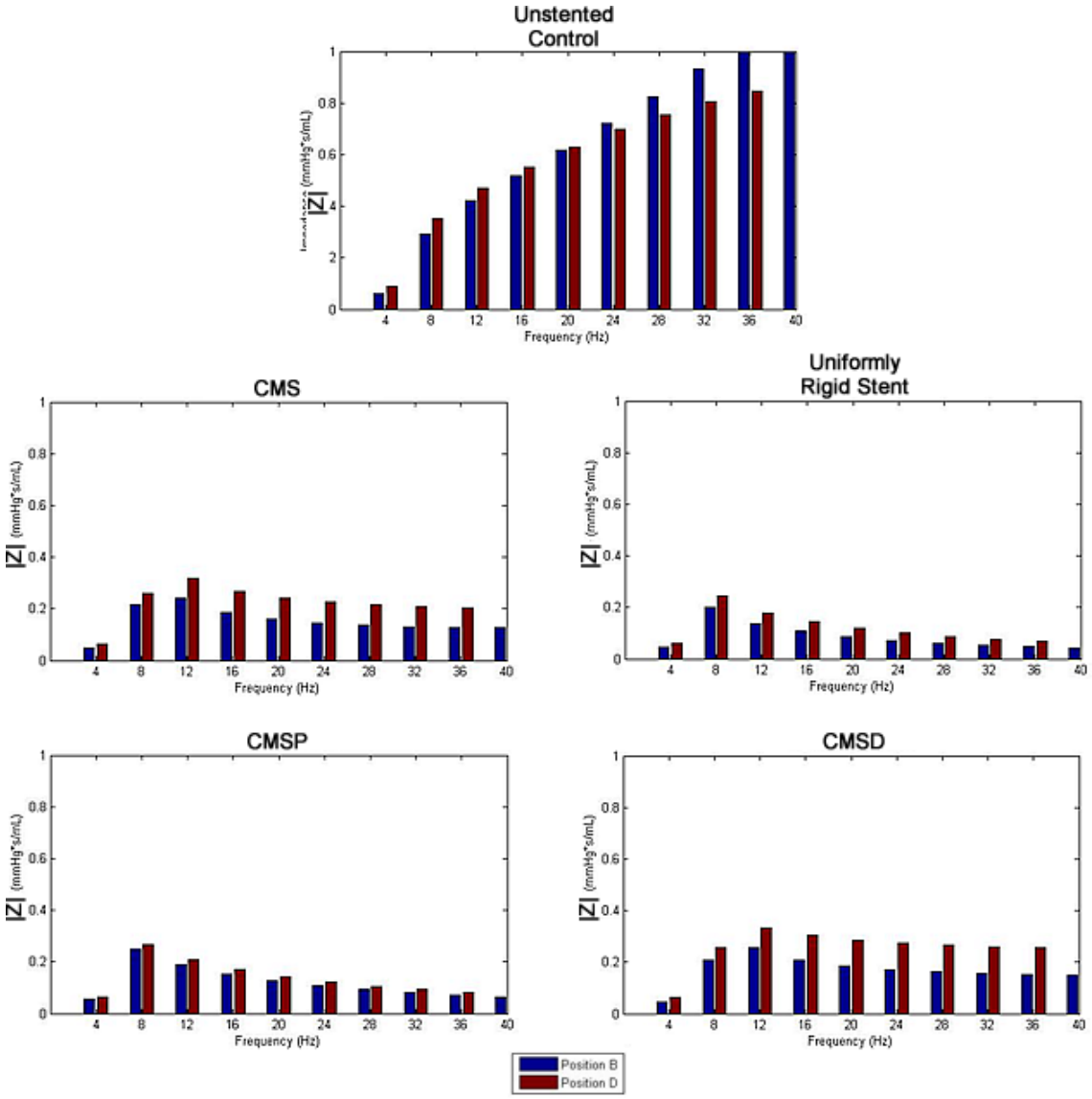

Fig. 14 Calculated |Z| in Relocated Stent Simulations. The results of the relocating the stent 5mm upstream of its original still showed a decrease in |Z| compared to our unstented control model. Subtle differences in |Z| were indicated by the Z_C calculations which could signify that a stent's location in reference to the origin has a very small impact on Z_C.

CHAPTER IV

SUMMARY AND CONCLUSIONS

Porcine model of PAH

As expected, the progression of pulmonary arterial hypertension alters the hemodynamics associated with the pulmonary vasculature, but it has yet to be determined whether these changes in turn continue to drive its progression. The development of the monocroatiline porcine PAH model analyzed in this study could be a valuable step toward better understanding the relationship between the progression of PAH and its associated hemodynamics. The increases in impedance found in this study parallel the hemodynamic changes seen in systemic hypertension [12,13] and in previous studies of PAH [26,27,28,29]. Since the Z_C is related to the compliance, cross sectional area, and wall thickness, the increase in Z_C would indicate possible changes in all three variables. Given the relationship between Z_C, compliance, (C) and area, (A), shown by

$$C = 2\pi r\left(\frac{\Delta r}{\Delta P}\right) \qquad (32)$$

$$Z_C = \sqrt{\frac{\rho \Delta P}{(\Delta A)A}} \qquad (33)$$

a decrease in the compliance of the pulmonary vasculature of vessel and in the total cross sectional area of the pulmonary vascular bed would both increase the Z_C. Furthermore, any increase in the thickness of the vessel walls would decrease compliance contributing to the observed elevated Z_C[26,28,29]. All of these changes in our model reflect the vascular remodeling occurring as the disease progresses [30]. The

muscularization of the smaller arterioles would decrease the total cross sectional area of the vascular bed causing an increase in Z_C and PVR. This migration/proliferation of smooth muscle cells into these tissues would also increase the thickness of the vessel walls, thereby decreasing the compliance and increasing Z_C. In addition, the strain stiffening characteristics of the arteries of the pulmonary vasculature would cause a decrease in compliance under the increased strain of a higher blood pressure. This result would be analogous to the increasing difficulty of inflating an already very inflated basketball compared to a less inflated one.

As with any study, there are limitations imposed upon the experiment by the model, and in this study it appears that the acquisition of the data could have had an impact on the data itself. Previous studies of PAH have utilized monocroatiline and rodent models [26,28,29], and other animal models have also been utilized to perform studies on other kinds of pulmonary hemodynamics [27], but, to the authors knowledge, this is the first attempt to use a full size, monocroatiline swine model under anesthesia. With this model, many parameters affect the acquisition of data and some of these parameters may be difficult to control while acquiring data. These parameters include the depth of anesthesia, the amount of saline administered to the animal, and the method used to mechanically open the chest to place the Q probe around the pulmonary artery.

Considering the difficulty in acquiring data, we recognized that the higher PVR and $\overline{P}$ seen in the control subjects (0.605±0.15 mmHg*s/mL and 34.1±2.0 mmHg,

respectively) could have been the result of the anesthesia or another contributing factor. The uncharacteristically high $\overline{P}$ and results of previous studies of the PAH indicate that the PVR should be elevated in the diseased subjects rather than the controls assuming the same body mass and blood Q through the pulmonary vasculature. This didn't appear to be the case in our analysis. However, we discovered that the hearts of the control animals were still maintaining a higher level of P_D and E_D per beat. This could be an indication of the health of the heart and lungs of these animals since they are still capable of sustaining an increased afterload and a short period of increased $\overline{P}$. This observation would also be consistent with the ability of a healthy right heart and lungs to withstand considerable preload, but at these elevated $\overline{P}$ these healthy hearts might be prone to dilation of the right ventricle [7,31].

Though unexpected [29], the apparent decreased PVR of the diseased animals in relation to the control could have occurred under a few specific situations. Originally, we considered side effects of the surgical procedure similar to those described above, but we also theorized that a more advanced diseased state and remodeled vasculature could have placed such an increased amount of stress on the heart that the subject was unable to maintain normal function. This idea was illustrated by the decreased P_D and E_D per beat seen in the diseased subjects. It was expected that a healthy animal would at least be capable of maintaining the same amount of P_D, despite a decreased E_D per beat, with an increase in heart rate similar to the one observed in DS4. However, this was not the case in the DS1, DS2, and DS3. Therefore, their hearts may not be capable of maintaining P_D.

In a second situation, we noted the observed changes in $\overline{P}$ and $\overline{Q}$ between the diseased and control subjects, and theorized that the animals were simply not capable of maintaining as much Q. In the diseased condition, we expect an increase in $\overline{P}$ assuming that the animal maintains $\overline{Q}$. However, if the animal isn't stressed, it seemed feasible that an animal would have a lower $\overline{P}$ corresponding to the diminished $\overline{Q}$. If this were the case, the diseased animals may have been physiologically sick compared to the controls and simply incapable of maintaining a high $\overline{P}$ or $\overline{Q}$ in the pulmonary vasculature.

In our final theory, we postulated that the animals were at a stage in the development of the disease where the diseased changes in the pulmonary vasculature have not yet become significant enough to increase $\overline{P}$ or PVR. The diseased subjects all had a higher |Z| and Z_C compared to the controls which would indicate that the pulmonary vasculature had begun remodeling, but a significant amount of remodeling may need to occur before an increase in $\overline{P}$ and PVR can be observed. This observation may be synonymous with undiagnosed early stages of the disease in humans where the symptoms haven't manifested enough to hinder normal everyday activities. Should this be the case early, noninvasive detection of changes in |Z| and Z_C may help to detect the development of PAH in individuals prone its development.

With the difficulty associated with acquiring data and the uncertainty of our results, it might be beneficial to utilize another method to measure the pulmonary blood Q and blood P for future studies of the hemodynamics associated with the advancement of PAH in a porcine model. A noninvasive method of measuring blood Q in addition to acquiring P with a pressure catheter would at least decrease the effects of saline administration and mechanically opening the chest. The measurement catheter would just need to be located within the vascular tree and the Q would need to be extracted from the same location via an imaging modality such as MRI or ultrasound. Another method to better study the hemodynamic effects and eliminate the effects of anesthesia might be to isolate and remove the system of interest completely for characterization. Such an approach would be very similar to those done in PAH studies by Chesler and colleagues [26,28,29], but this approach may be more difficult given a swine's size compared to those of mice.

Ability of a stent to alter wave propagation

Our simplified models of a stented vessel indicate that stents do alter wave propagation in vessels. Given our PAH analysis and the calculations of forward and backward running waves, we focused much of our analysis on the |Z| and Z_C of the different models, and we came to realize that a decrease in the |Z| and Z_C would be the desired result of applying a stent. Our stent models demonstrated that the stents are capable of achieving this objective. They also indicated that the each stent design had a slightly different effect than the other stent designs. However, despite the changes in the |Z| and

Z_C, a large difference between the proximal and distal ends of the vessel would need to be observed to indicate the presence of a filtering characteristic in a stent. This large difference would imply that a physiological signal is being prevented from returning past the stent from the periphery. All of the stents models showed that the stents increased the difference between the proximal and distal Z_C compared to our unstented control. Specifically, the uniformly rigid stent created the least amount of difference between our measurement locations, and the CMSP model appeared to create the greatest amount of difference. This observation with our first set of simulations and the cosine simulations could indicate that the compliant end allows for the easy transfer of energy across the stent while the sharp contrast at the rigid end serves to prevent its return. Yet, these results can't be conclusive. The difference in proximal and distal Z_C in our third, relocated stent simulations contradicted the other two. It originally appeared that this phenomenon was caused by moving the location of the stent relative to the origin. The more likely cause though was moving of the stent relative to the measurement point B and point D. In this simulation, point B would have ended up inside of the stent which would have increased the dependence of Z_C on the mechanical properties [25] of the stent rather than any changes reflections, Q, or P.

Ability of a stent to mediate disease progression

Even with these results, the application of a stent to mediate disease progression or to alter the hemodynamics associated with a progressive disease such a PAH or bronchopulmonary dysplasia would be an attempt to apply a local solution to a global

problem. In our results, we had hoped to see a major changes between the proximal and distal measurements, but the changes in amplitude and small changes in wave profile were likely not sufficient to provoke the intended global response or to alleviate disease progression given the size of the model. Furthermore, the original intent of the deployment of a stent has a local focus. As such, its designs were and still are driven by the local environment associated with a stenosis, balloon angioplasty, and the complications of previously failed stenting. The issues in their designs coupled with current complications seen in angioplasty and associated with stent restenosis currently make an application outside its original intent to provide a serve as a scaffold for vascular healing risky and unnecessary.

Moreover, from an engineering standpoint, a stent is small compared to the wavelength of P and Q. Studies have shown that the effects of elastic nonuniformities are small given long wavelengths [32]. Therefore, the size of a stent should make its application as a filter small, and its effects on the impedance of a more complex system would be relatively negligible compared to the effects of bifurcations, pathlengths, or vascular constriction.

Limitations and future directions

Many limitations, assumptions, and restrictions impeded our analysis and the development of more conclusive theories. One of the larger of these assumptions was the size of the vessel and the size of the stent. The ratio between the size of the stent and the

size of the modeled vessel was quite a bit larger than it would be in a physiological setting, and, had the model been non-dimensionalized or enlarged, this simulation may have provided a better simulation for the application of a graft. Given this observation, we considered altering the length of the vessel and the models dimensions because the length might more adequately compare to the wavelength of a vessel. Yet such results were beyond the scope of the project.

Our model's design however was restricted most by the derivation of the wave equation and its assumptions: a straight, compliant tube, an inviscid fluid, small deformations, linear elasticity, and a wave speed much larger than blood velocity ($c>>u$). The most significant of these assumptions was the geometric straight tube assumption. Physiologically, a vessel would only be straight over a very short distance. Thus we restricted our vessel to a length of 5 mm, but, in hindsight, we would have preferred to add vessel tapering and bifurcations to more adequately simulate a stent in a bifurcating vascular system. These additions proved to be difficult though because of the linear, straight tube assumptions.

Many changes could have been made to our original model design which could have led to more conclusive results. Most importantly, a more adequate non-linear model with bifurcations and vessel tapering would have had a profound influence on our results. Vessel bifurcations and tapering should have improved the frequency content of our calculated |P|, |Q|, and |Z| which, in turn, would have allowed us to better analyze a

stent's ability to filter higher frequency content. To create such a complex, adequate system with bifurcations, vessel tapering, and a stented region, it may be required to use nonlinear equations and computational methods. Studies have already shown that nonlinear models are very capable of modeling the human vasculature [33,34] and blood flow [21], and some of the results of these simulations have even be validated by in vitro experiments [34,35]. Specifically, recent work by Matthys et al [34] have shown the accuracy of non-linear 1-D computational vascular networks. An adaptation to this model by adding a stiffer less elastic region (a stent) could easily address our original questions in a systemic vasculature setting. For the sake of completeness, a model similar to theirs could also be adapted to simulate the pulmonary vasculature. One could even validate such a model with in vitro testing which is something that has, to the author's knowledge, yet to be done. Also, multiple mathematical models of the pulmonary vasculature currently exist [36] which could help expedite such an investigation.

A final review of our simulation also noted our emphasis on the increased stiffness of a vessel with a stent, but it might be beneficial to investigate this phenomenon with a region of increased compliance. We chose to focus our study on the application of a stent because of its abundance of use in cardiovascular treatment. Considering the application of a device which restores or enhances the compliance of a vessel may produce contradictory or improved results. In theory, a more compliant region could create reservoir or an area in which to story energy within the vasculature. In turn, this

area could provide a cushion for disturbances and reflections propagating back from the periphery.

Conclusions

This porcine model of PAH could be valuable to improving our understanding of the progression of PAH and to evaluate therapeutic options, but more research will need to be devoted to establishing the connection between hemodynamics and the progression of PAH in this model. However, we did identify changes in |Z| and Z_C in the disease animals, and, since our stent models altered |Z| and Z_C, it appeared that stents have an impact on wave propagation in a small vessel. Still, the small changes in P and Q produced by the stent, the small size of the stent in comparison to the wavelength, and stent complications indicated that a stent would probably not invoke the global response necessary to affect the progression of PAH or BPD.

REFERENCES

[1] Rolland, P.-H., Lagausie, P. d., Stathopoulos, E., Lepre`tre, O., Viudes, G., Gorincour, G., Hery, G. r., Magne´e, C. d., Paut, O., and Guys, J.-M., 2008, "Phasic Hemodynamics and Reverse Blood Flows in the Aortic Isthmus and Pulmonary Arteries of Preterm Lambs with Pulmonary Vascular Dysfunction," Am. J. of Physiol Heart Circ Physiol, **295**, p. 2231-2241.

[2] Jobe, A. H., and Bancalari, E., 2001, "Bronchopulmonary Dysplasia," Am. J. Respir. Crit. Care Med., **163**(7), pp. 1723-1729.

[3] Stenmark, K. R., and Abman, S. H., 2005, "Lung Vascular Development: Implications for the Pathogenesis of Bronchopulmonary Dysplasia," Ann. Rev. Physiol., **67**, pp. 623-661.

[4] Shehata, S. M., Tibboel, D., Sharma, H. S., and Mooi, W. J., 1999, "Impaired Structural Remodelling of Pulmonary Arteries in Newborns with Congenital Diaphragmatic Hernia: a Histological Study of 29 Cases," J. Pathol., **189**(1), pp. 112-118.

[5] American Heart Association, "Primary or Unexplained Pulmonary Hypertension," 2008, http://www.americanheart.org/presenter.jhtml?identifier=4752.

[6] Mandel, J., and Taichman, D., c2006, *Pulmonary Vascular Disease /* edited by Jess Mandel, Darren Taichman, Saunders/Elsevier, Philadelphia.

[7] Hill, N. S., MD, and Farber, H. W., MD, 2008, *Pulmonary Hypertension*, Humana Press, Totowa, NJ.

[8] Said, S. I., 2006, "Mediators and Modulators of Pulmonary Arterial Hypertension," Am. J. Physiol. Lung Cell. Mol. Physiol., **291**(4), pp. L547-558.

[9] D'Alonzo, G. E., Barst, R. J., Ayres, S. M., Bergofsky, E. H., Brundage, B. H., Detre, K. M., Fishman, A. P., Goldring, R. M., Groves, B. M., and Kernis, J. T., 1991, "Survival in Patients with Primary Pulmonary Hypertension. Results from a National Prospective Registry," Ann. Intern Med, **115**(5), pp. 343-349.

[10] American Lung Association, "Primary Pulmonary Hypertension (PPH) Fact Sheet," 2003, http://www.lungusa.org/site/apps/nlnet/content3.aspx?c=dvLUK9O0E&b=2060321&content_id={FA692DC0-B9A9-4BDC-88F4-2609BD6E0EDD}&notoc=1.

[11] White, R. J., Meoli, D. F., Swarthout, R. F., Kallop, D. Y., Galaria, II, Harvey, J. L., Miller, C. M., Blaxall, B. C., Hall, C. M., Pierce, R. A., Cool, C. D., and Taubman, M. B., 2007, "Plexiform-Like Lesions and Increased Tissue Factor Expression in a Rat Model of Severe Pulmonary Arterial Hypertension," Am. J. Physiol Lung Cell Mol Physiol, **293**(3), pp. L583-590.

[12] Li, J. K. J., 2000, *The Arterial Circulation : Physical Principles and Clinical Applications*, Humana Press, Totowa, N.J.

[13] Westerhof, N., Stergiopulos, N., and Noble, M. I. M., 2005, *Snapshots of Hemodynamics : An Aid for Clinical Research and Graduate Education*, Springer, New York.

[14] Bleecker, D., and Csordas, G., 1992, *Basic Partial Differential Equations*, Van Nostrand Reinhold, New York.

[15] Nagle, R. K., Saff, E. B., and Snider, A. D., 2004, *Differential Equations and Boundary Value Problems*, Pearson Custom Publishing, Boston, MA.

[16] American Heart Association, "Cardiovascular Disease Statistics," 2008, http://www.americanheart.org/presenter.jhtml?identifier=4478.

[17] Wyatt, M. G., and Watkinson, A. F. A. F., c2006, *Endovascular Therapies /* Edited by Michael G. Wyatt and Anthony F. Watkinson., TFM Publishing, Shrewsbury, UK

[18] Bedoya, J., Meyer, C. A., Timmins, L. H., Moreno, M. R., and Moore, J. E., 2006, "Effects of Stent Design Parameters on Normal Artery Wall Mechanics," ASME J. of Biomech. Eng, **128**(5), pp. 757-765.

[19] Berry, J. L., Manoach, E., Mekkaoui, C., Rolland, P. H., Moore, J. E., Jr., and Rachev, A., 2002, "Hemodynamics and Wall Mechanics of a Compliance Matching Stent: In Vitro and In Vivo Analysis," J. Vasc. Interv. Radiol., **13**(1), pp. 97-105.

[20] Quick, C. M., Berger, D. S., and Noordergraaf, A., 2001, "Constructive and Destructive Addition of Forward and Reflected Arterial Pulse Waves," Am. J. Physiol - Heart Circ. Physiol., **280**(4), pp. H1519-1527.

[21] Humphrey, J. D., 2002, *Cardiovascular Solid Mechanic : Cells, Tissues, and Organs*, Springer, New York.

[22] Wan, J., Steele, B., Spicer, S. A., Strohband, S., Feijoo, G. R., Hughes, T. J., and Taylor, C. A., 2002, "A One-Dimensional Finite Element Method for

Simulation-Based Medical Planning for Cardiovascular Disease," Computer Methods in Biomechanics & Biomedical Engineering, **5**(3), pp. 195-206.

[23] Altman, P. L., and Katz, D. D., 1971, *Respiration and Circulation*, Federation of American Societies for Experimental Biology, Bethesda, MD.

[24] Reddy, J. N., 1993, An *Introduction to the Finite Element Method*, MacGraw Hill, Boston.

[25] Pythoud, F., Stergiopulos, N., and Meister, J. J., 1996, "Separation of Arterial Pressure Waves into Their Forward and Backward Running Components," ASME J. Biomech. Eng., **118**(3), pp. 295-301.

[26] Kobs, R. W., Muvarak, N. E., Eickhoff, J. C., and Chesler, N. C., 2005, "Linked Mechanical and Biological Aspects of Remodeling in Mouse Pulmonary Arteries with Hypoxia-Induced Hypertension," Am J Physiol Heart Circ Physiol, **288**(3), pp. H1209-1217.

[27] Kussmaul, W. G., Noordergraaf, A., and Laskey, W. K., 1992, "Right Ventricular-Pulmonary Arterial Interactions," Ann. Biomed. Eng., **20**(1), pp. 63-80.

[28] Tuchscherer, H. A., Webster, E. B., and Chesler, N. C., 2006, "Pulmonary Vascular Resistance and Impedance in Isolated Mouse Lungs: Effects of Pulmonary Emboli," Ann. Biomed. Eng., **34**(4), pp. 660-668.

[29] Tuchscherer, H. A., Vanderpool, R. R., and Chesler, N. C., 2007, "Pulmonary Vascular Remodeling in Isolated Mouse Lungs: Effects on Pulsatile Pressure-Flow Relationships," J. Biomech., **40**(5), pp. 993-1001.

[30] Humbert, M., Morrell, N. W., Archer, S. L., Stenmark, K. R., MacLean, M. R., Lang, I. M., Christman, B. W., Weir, E. K., Eickelberg, O., Voelkel, N. F., and Rabinovitch, M., 2004, "Cellular and Molecular Pathobiology of Pulmonary Arterial Hypertension," JACC, **43**(12 Suppl S), pp. 13S-24S.

[31] Bristow, M. R., Zisman, L. S., Lowes, B. D., Abraham, W. T., Badesch, D. B., Groves, B. M., Voelkel, N. F., Lynch, D. M., and Quaife, R. A., 1998, "The Pressure-Overloaded Right Ventricle in Pulmonary Hypertension," Chest, **114**(1 Suppl), pp. 101S-106S.

[32] Taylor, M. G., 1966, "The Input Impedance of an Assembly of Randomly Branching Elastic Tubes," Biophysical journal, **6**(1), pp. 29-51.

[33] Vignon, I. E., and Taylor, C. A., 2004, "Outflow Boundary Conditions for One-Dimensional Finite Element Modeling of Blood Flow and Pressure Waves in Arteries," Wave Motion, **39**, pp. 361-374.

[34] Matthys, K. S., Alastruey, J., Peiro, J., Khir, A. W., Segers, P., Verdonck, P. R., Parker, K. H., and Sherwin, S. J., 2007, "Pulse Wave Propagation in a Model Humkan Arterial Network: Assessment of 1-D Numerical Simulations Against In Vitro Measurements," J. of Biomech, **40**, pp. 3476-3486.

[35] Nichols, W. W., and O'Rourke, M. F., 1990, *McDonald's Blood Flow in Arteries Theoretic, Experimental and Clinical Principles*, Third edition, Lea & Febiger, Philadelphia, PA.

[36] Wiener, F., Morkin, E., Skalak, R., and Fishman, A., 1966, "Wave Propagation in the Pulmonary Circulation," Circ. Res., **XIX**(October), pp. 834-850.

CONTACT INFORMATION

Name:	Andrew Milton Peters
Professional Address:	c/o Dr. James E. Moore, Jr. Department of Biomedical Engineering 337 Zachry Engineering Center Texas A&M University College Station, TX 77843-3120
Email Address:	andrewpeters09@tamu.edu
Education:	B.S., Biomedical Engineering, Texas A&M University May 2009 Magna Cum Laude Undergraduate Research Scholar Alpha Eta Mu Beta